Eur. Phys. J. C 47, 703–721 (2006)
Digital Object Identifier (DOI) 10.1140/epjc/s2006-02608-5

THE EUROPEAN PHYSICAL JOURNAL C

On the scale variation of the total cross section for Higgs production at the LHC and at the Tevatron

A. Cafarella[1,2,a], C. Corianò[1,b], M. Guzzi[1,c], J. Smith[3,4,d]

[1] Dipartimento di Fisica, Università di Lecce and INFN sezione di Lecce, Via per Arnesano, 73100 Lecce, Italy
[2] Department of Physics, University of Crete, 71003 Heraklion, Greece
[3] C.N. Yang Institute for Theoretical Physics, State University of New York at Stony Brook, New York 11794-3840, USA
[4] NIKHEF, Postbus 41882, 1009 DB, Amsterdam, The Netherlands

Received: 17 October 2005 / Revised version: 18 May 2006 /
Published online: 21 July 2006 –

Abstract. We present a detailed study of the total pp cross section for scalar Higgs production to next-to-next-to-leading order in α_s at LHC energies, and of the $p\bar{p}$ cross section at the Tevatron, combining an implementation of the solutions of the parton evolution equations at the three-loop order with the corresponding hard scatterings, evaluated at the same perturbative order. Our solutions of the DGLAP equations are implemented directly in x-space and allow for the study of the dependence of the results on the factorization (μ_F) and renormalization scales (μ_R) typical of a given process, together with the stability of the perturbative expansion. The input sets for the parton evolutions are those given by Martin, Roberts, Stirling and Thorne and by Alekhin. Results for K-factors are also presented. The NNLO corrections can be quite sizeable at typical collider energies. The stability region of the perturbative expansion is found when $\mu_R > m_H \sim \mu_F$.

1 Introduction

The validity of the mechanism of mass generation in the standard model will be tested at the new collider, the LHC. For this we require precision studies in the Higgs sector to confirm its existence. This program involves a rather complex analysis of the QCD backgrounds with the corresponding radiative corrections fully taken into account. Studies of these corrections for specific processes have been performed by various groups, to an accuracy which has reached the next-to-next-to-leading order (NNLO) level in α_s, the QCD coupling constant. The quantification of the impact of these corrections requires the determination of the hard scattering partonic cross sections up to order α_s^3, together with the DGLAP kernels controlling the evolution of the parton distributions determined at the same perturbative order. Therefore, the study of the evolution of the parton distributions, using the three-loop results on the anomalous dimensions [1], is critical for the success of this program. Originally NNLO predictions for some particular processes such as total cross sections [2] have been obtained using the approximate expressions for these kernels [3]. The completion of the exact computation of the NNLO DGLAP kernels motivates more detailed studies of the same observables based on these exact kernels and the investigation of the factorization (μ_F) and renormalization (μ_R) scale dependences of the result, which are still missing. In this work we are going to reanalyze these issues from a broader perspective. Our analysis is here exemplified in the case of the total cross sections at the LHC (pp) and at the Tevatron ($p\bar{p}$) for Higgs production using the hard scatterings computed in [2] and their dependence on the factorization and renormalization scales. Our study is based on the exact and well defined NNLO computations of the hard scatterings for this process and we have not taken into account any threshold resummation since this involves further approximations. These effects have been considered in [4]. The DGLAP equation is solved directly in x-space using a method which is briefly illustrated below and which is accurate up to order α_s^2. Our input distributions at a small scale will be specified below. We also analyze the corresponding K-factors and the region of stability of the perturbative expansion by studying their variation under changes in all the relevant scales. It is shown that the NNLO corrections are sizeable while the region of reduced scale dependence is near the value $\mu_F = m_H$ with μ_R around the same value but slightly higher.

2 Higgs production at LHC

The Higgs field, being responsible for the mechanism of mass generation, can be radiated off by any massive state and its coupling is proportional to the mass of the same

[a] e-mail: alessandro.cafarella@le.infn.it
[b] e-mail: claudio.coriano@le.infn.it
[c] e-mail: marco.guzzi@le.infn.it
[d] e-mail: smith@insti.physics.sunysb.edu

state. At the LHC one of the golden plated modes to search for the Higgs is its production via the mechanism of gluon fusion. The leading order contribution is shown in Fig. 1 which shows that dependence of the amplitude is through the quark loop. Most of the contribution comes from the top quark, since this is the heaviest quark and has the largest coupling to the Higgs field. NLO and NNLO corrections have been computed in the last few years by various groups [5], [6]. A typical NLO correction is shown in Fig. 2. In the infinite mass limit of the quark mass in the loop (see [7] for a review), an effective description of the process is obtained in leading order by the Lagrangian density

$$\begin{aligned}\mathcal{L}_{\rm eff} &= \frac{\alpha_{\rm s}}{12\pi} G^A_{\mu\nu} G^{A\ \mu\nu} \left(\frac{H}{v}\right) \\ &= \frac{\beta_{\rm F}}{g_{\rm s}} G^A_{\mu\nu}\ G^{A\ \mu\nu} \left(\frac{H}{2v}\right)(1-2\alpha_{\rm s}/\pi),\end{aligned}$$

with

$$\beta_{\rm F} = \frac{g_{\rm s}^3 N_{\rm H}}{24\pi^2} \tag{1}$$

being the contribution of $N_{\rm H}$ heavy fermion loops to the QCD beta function. This effective Lagrangian can be used to compute the radiative corrections in the gluon sector. A discussion of the NNLO approach to the computation of the gluon fusion contributions to Higgs production has been presented in [2], to which we refer for more details. We recall that in this paper the authors presented a study for both scalar and pseudoscalar Higgs production, the pseudoscalar appearing in two-Higgs doublets models. The diagonalization of the mass matrix for the Higgs at the minimum introduces scalar and pseudoscalar interactions between the various Higgs and the quarks, as shown from the structure of the operator O_2 below in (3). In the large top-quark mass limit the Feynman rules for scalar Higgs production (H) can be derived from the effective Lagrangian density [8–10],

$$\mathcal{L}^{\rm H}_{\rm eff} = G_{\rm H} \Phi^{\rm H}(x) O(x) \quad \text{with} \quad O(x) = -\frac{1}{4} G^a_{\mu\nu}(x) G^{a,\mu\nu}(x), \tag{2}$$

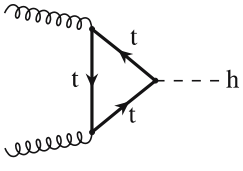

Fig. 1. The leading order diagram for Higgs production by gluon fusion

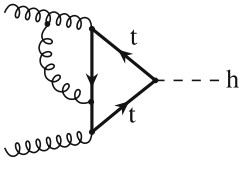

Fig. 2. A typical NLO diagram for Higgs production by gluon fusion

whereas the production of a pseudoscalar Higgs [11] (A) is obtained from

$$\begin{aligned}\mathcal{L}^{\rm A}_{\rm eff} &= \Phi^{\rm A}(x)\left[G_{\rm A} O_1(x) + \tilde{G}_{\rm A} O_2(x)\right] \quad \text{with} \\ O_1(x) &= -\frac{1}{8}\epsilon_{\mu\nu\lambda\sigma} G^{\mu\nu}_a G^{\lambda\sigma}_a(x)\,, \\ O_2(x) &= -\frac{1}{2}\partial^\mu \sum_{i=1}^{n_f} \bar{q}_i(x)\gamma_\mu\gamma_5 q_i(x)\,,\end{aligned} \tag{3}$$

where $\Phi^{\rm H}(x)$ and $\Phi^{\rm A}(x)$ represent the scalar and pseudoscalar fields respectively and n_f denotes the number of light flavors. $G^{\mu\nu}_a$ is the field strength of QCD and the quark fields are denoted by q_i. We refer the reader to [2] for further details.

Using the effective Lagrangian one can calculate the total cross section of the reaction

$$H_1(P_1) + H_2(P_2) \to {\rm B} + X\,, \tag{4}$$

where H_1 and H_2 denote the incoming hadrons and X represents an inclusive hadronic state and B denotes the scalar or the pseudoscalar particle produced in the reaction. The total cross section is given by

$$\begin{aligned}\sigma_{\rm tot} = &\frac{\pi G^2_{\rm B}}{8(N^2-1)} \\ &\times \sum_{a,b=q,\bar{q},g} \int_x^1 {\rm d}x_1 \int_{x/x_1}^1 {\rm d}x_2 f_a\left(x_1,\mu^2\right) f_b\left(x_2,\mu^2\right) \\ &\times \Delta_{ab,{\rm B}}\left(\frac{x}{x_1 x_2}, \frac{m^2}{\mu^2}\right)\,, \\ \text{with } x = &\frac{m^2}{S}\,, S = (P_1+P_2)^2\,,\end{aligned} \tag{5}$$

where the factor $1/(N^2-1)$ is due to the average over color. The parton distributions $f_a(y,\mu^2)$ $(a, b = q, \bar{q}, g)$ depend on the mass factorization/renormalization scale μ. $\Delta_{ab,{\rm B}}$ denotes the partonic hard scattering coefficient computed with NNLO accuracy.

3 The NNLO evolution

We summarize the main features of the NNLO DGLAP evolution. As usual we introduce singlet (+) and non-singlet (−) parton distributions

$$q_i^{(\pm)} = q_i \pm \overline{q}_i, \quad q^{(\pm)} = \sum_{i=1}^{n_f} q_i^{(\pm)}, \tag{6}$$

whose evolution is determined by the corresponding equations:

$$\begin{aligned}&\frac{\rm d}{{\rm d}\log Q^2}\begin{pmatrix} q^{(+)}(x,Q^2) \\ g(x,Q^2)\end{pmatrix} = \\ &\begin{pmatrix} P_{qq}\left(x,\alpha_s(Q^2)\right) P_{qg}\left(x,\alpha_s(Q^2)\right) \\ P_{gq}\left(x,\alpha_s(Q^2)\right) P_{gg}\left(x,\alpha_s(Q^2)\right)\end{pmatrix} \otimes \begin{pmatrix} q^{(+)}(x,Q^2) \\ g(x,Q^2)\end{pmatrix}\end{aligned} \tag{7}$$

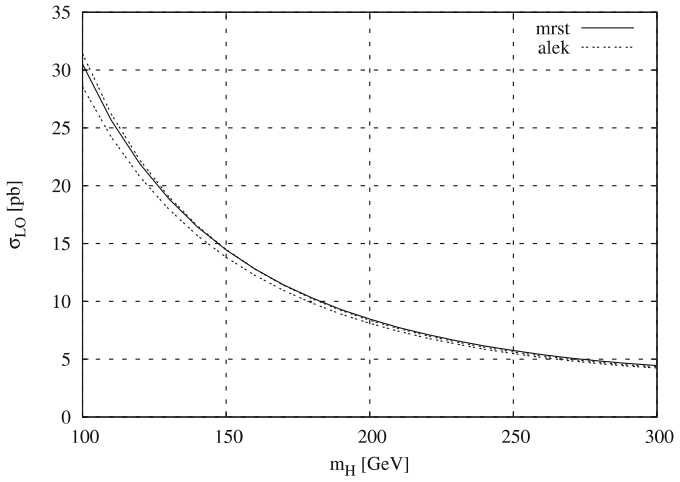

(a) LHC

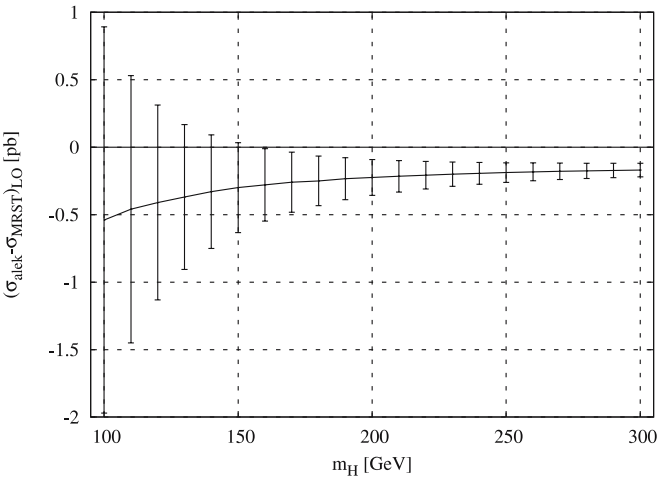

(b) LHC

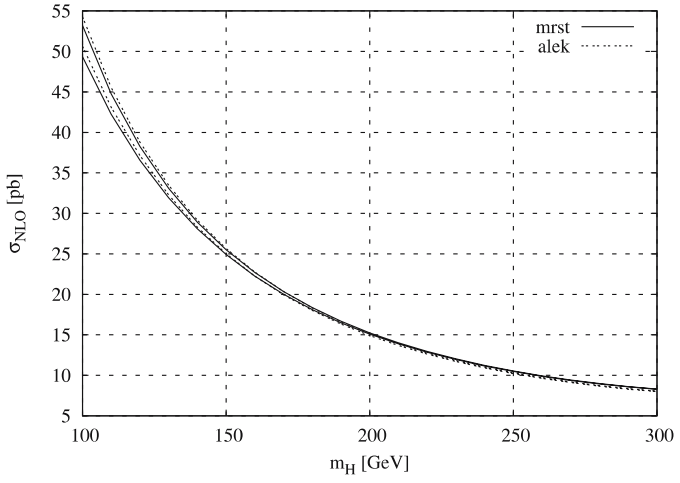

(c) LHC

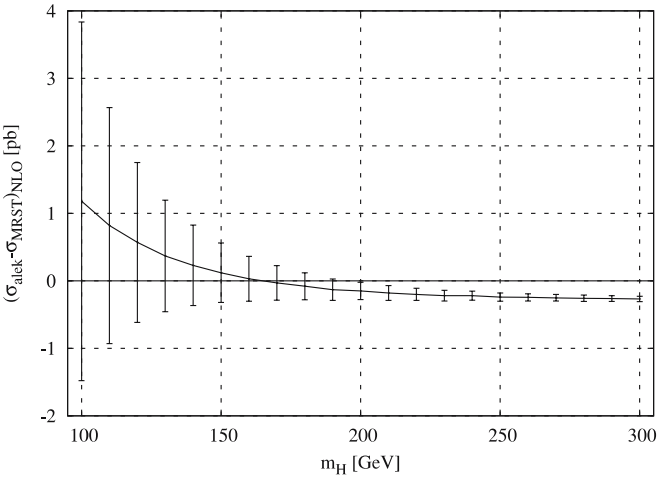

(d) LHC

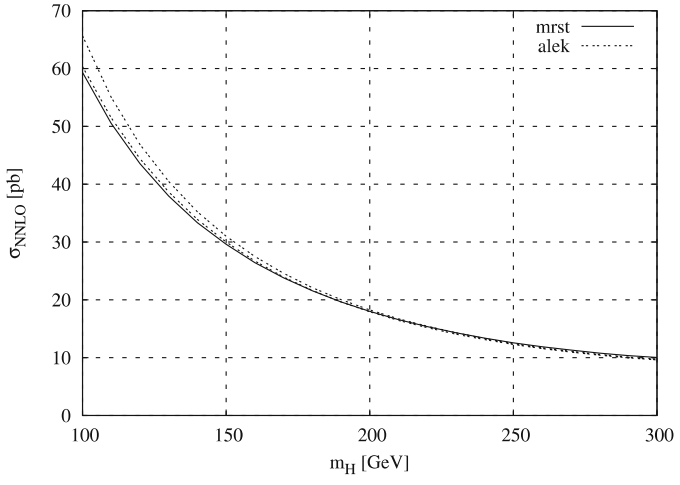

(e) LHC

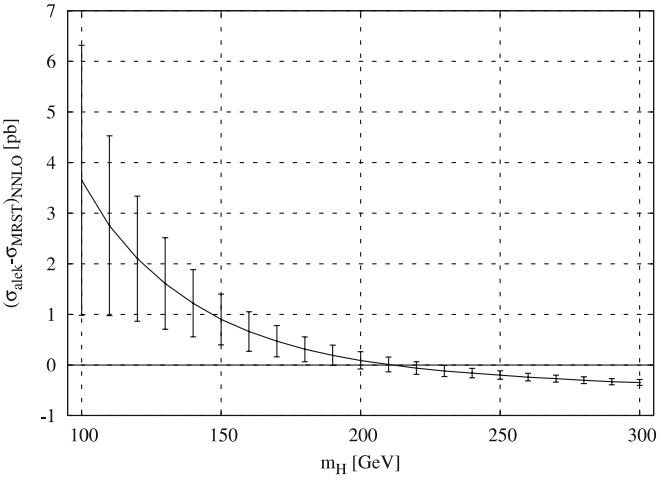

(f) LHC

Fig. 3. Cross sections for the scalar Higgs production at the LHC with $\mu_{\rm R}^2 = \mu_{\rm F}^2 = m_H^2$. When available (Alekhin at all orders and MRST at NLO) the error bands are shown. See Sect. 5 for comments

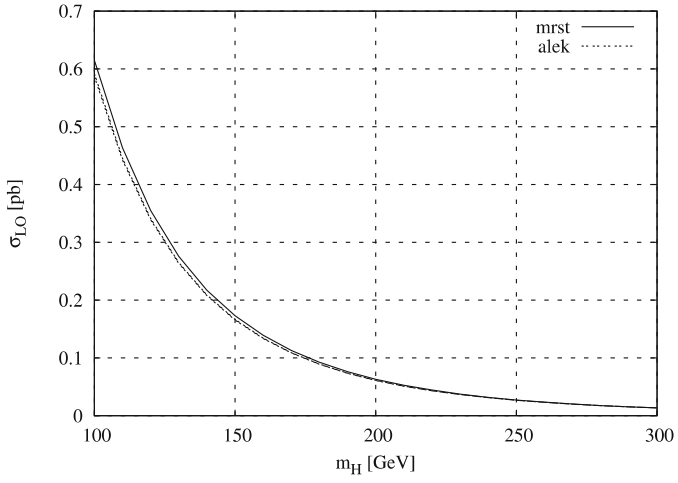

(a) Tevatron

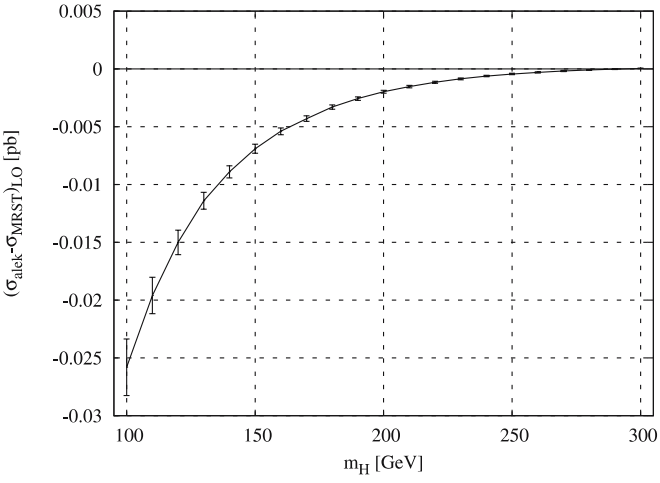

(b) Tevatron

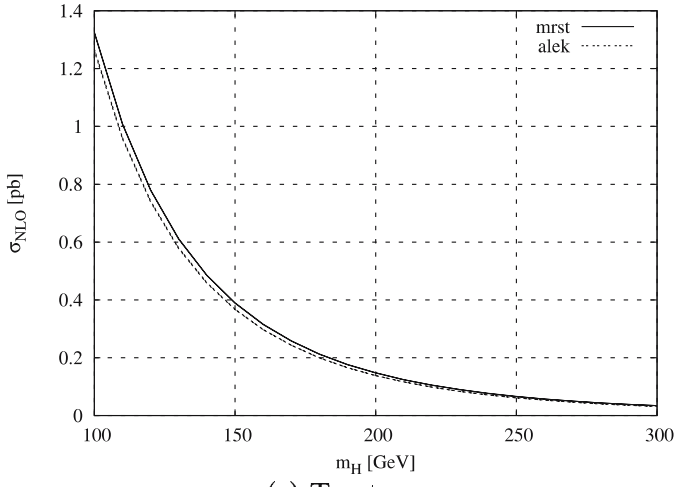

(c) Tevatron

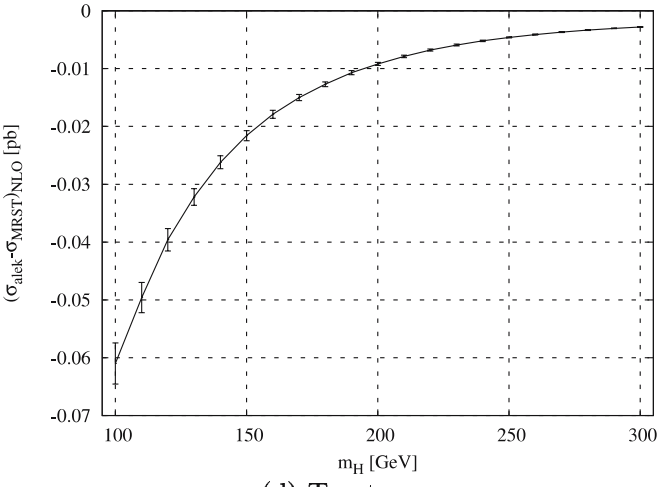

(d) Tevatron

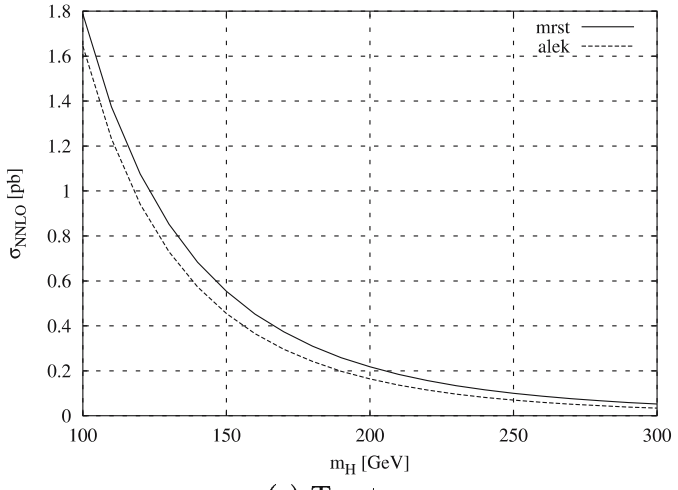

(e) Tevatron

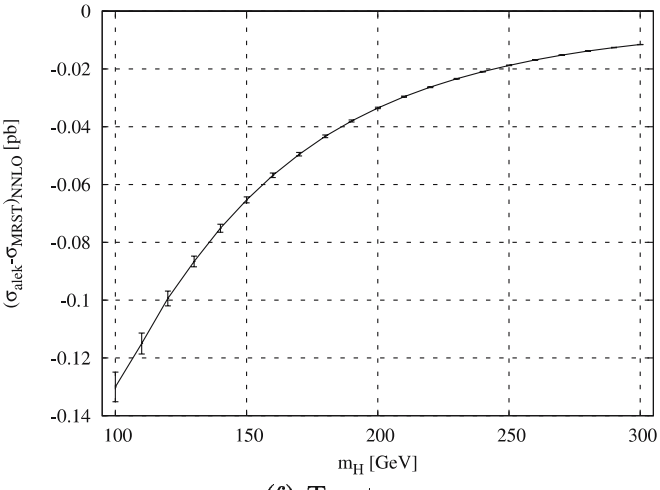

(f) Tevatron

Fig. 4. Like in Fig. 3 but for the Tevatron. In **a**, **c** and **e** the error bands are so tiny that the lines look superimposed

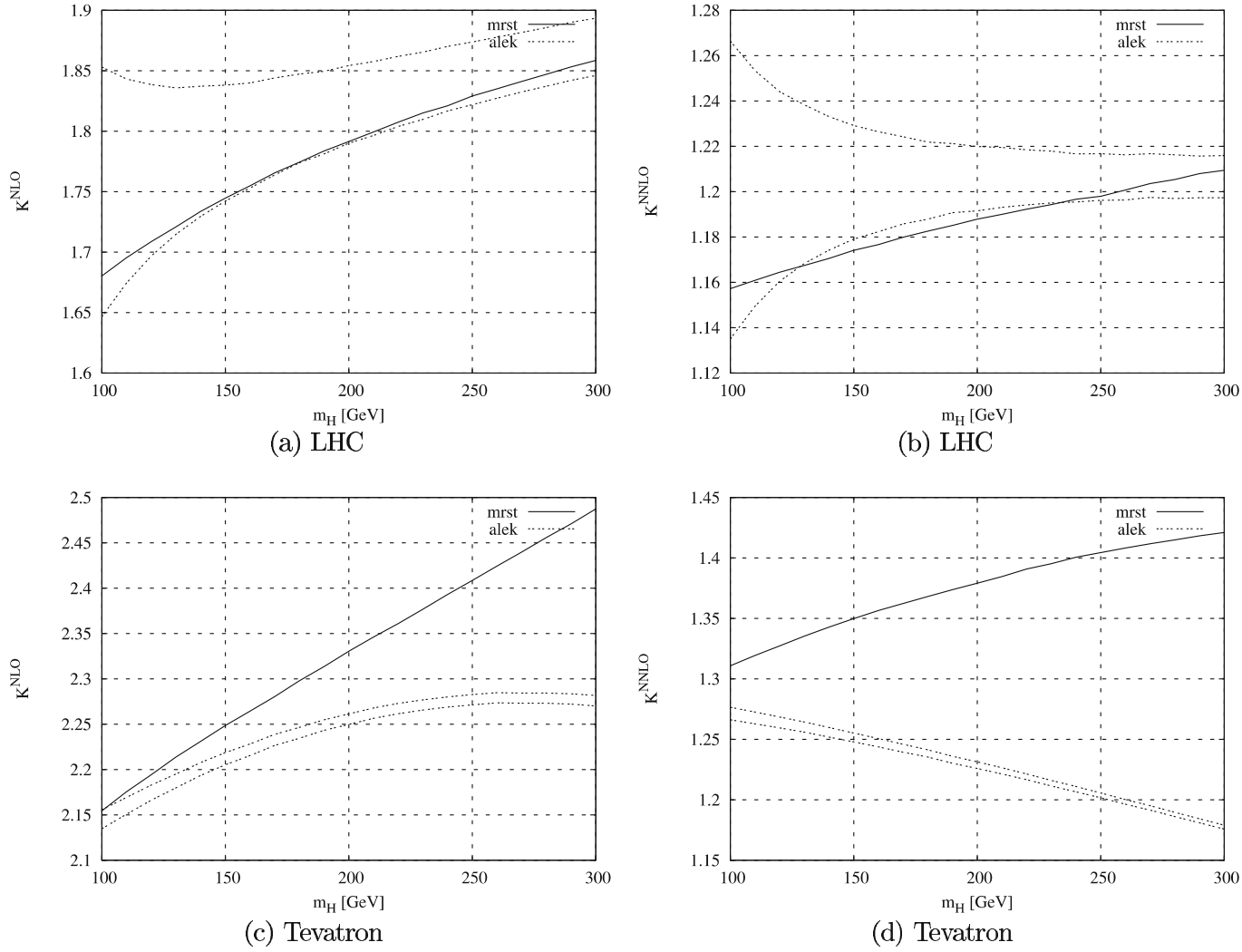

Fig. 5. K-factors for the scalar Higgs at NNLO/NLO and NLO/LO with $\mu_{\rm R}^2 = \mu_{\rm F}^2 = m_H^2$. When available (Alekhin at all orders and MRST at NLO) the error bands are shown

for the singlet combination, and a scalar one for the non-singlet case:

$$\frac{\mathrm{d}}{\mathrm{d}\log Q^2} q_i^{(-)}(x,Q^2) = P_{\rm NS}\left(x,\alpha_s(Q^2)\right) \otimes q_i^-(x,Q^2)\,. \quad (8)$$

The convolution product is defined by

$$[a\otimes b]\,(x) = \int_x^1 \frac{\mathrm{d}y}{y} a\left(\frac{x}{y}\right) b(y) = \int_x^1 \frac{\mathrm{d}y}{y} a(y) b\left(\frac{x}{y}\right)\,. \quad (9)$$

We recall that the perturbative expansion, up to NNLO, of the kernels is

$$P(x,a_s) = a_{\rm s} P^{(0)}(x) + a_{\rm s}^2 P^{(1)}(x) + a_{\rm s}^3 P^{(2)}(x) + \ldots \quad (10)$$

where $a_{\rm s} \equiv \alpha_{\rm s}/(4\pi)$. In order to solve the evolution equations directly in x-space [12, 13], (see [14] for an NLO implementation of the method), we assume solutions of the form [15]

$$f(x,Q^2) = \sum_{n=0}^{\infty} \frac{A_n(x)}{n!} \log^n \frac{a_s(Q^2)}{a_s(Q_0^2)} + a_{\rm s}(Q^2) \sum_{n=0}^{\infty} \frac{B_n(x)}{n!} \log^n \frac{a_s(Q^2)}{a_s(Q_0^2)} + a_s^2(Q^2) \sum_{n=0}^{\infty} \frac{C_n(x)}{n!} \log^n \frac{a_s(Q^2)}{a_s(Q_0^2)} \quad (11)$$

for each parton distribution f, where Q_0 defines the initial evolution scale. The ansatz is introduced into the evolution equations and used to derive recurrence relations for its unknown coefficients A_n, B_n, C_n, involving polylogarithmic functions [16, 17] which are then implemented numerically.

This ansatz corresponds to a solution of the DGLAP equation accurate up to order $a_{\rm s}^2$ (truncated solution). It can be shown that [15] this ansatz reproduces the solution of the DGLAP equation in (Mellin) moment space obtained with the same accuracy in $a_{\rm s}$. Modifications of this ansatz also allow one to obtain the so-called "exact" solutions of the equations for the moments [18]. These sec-

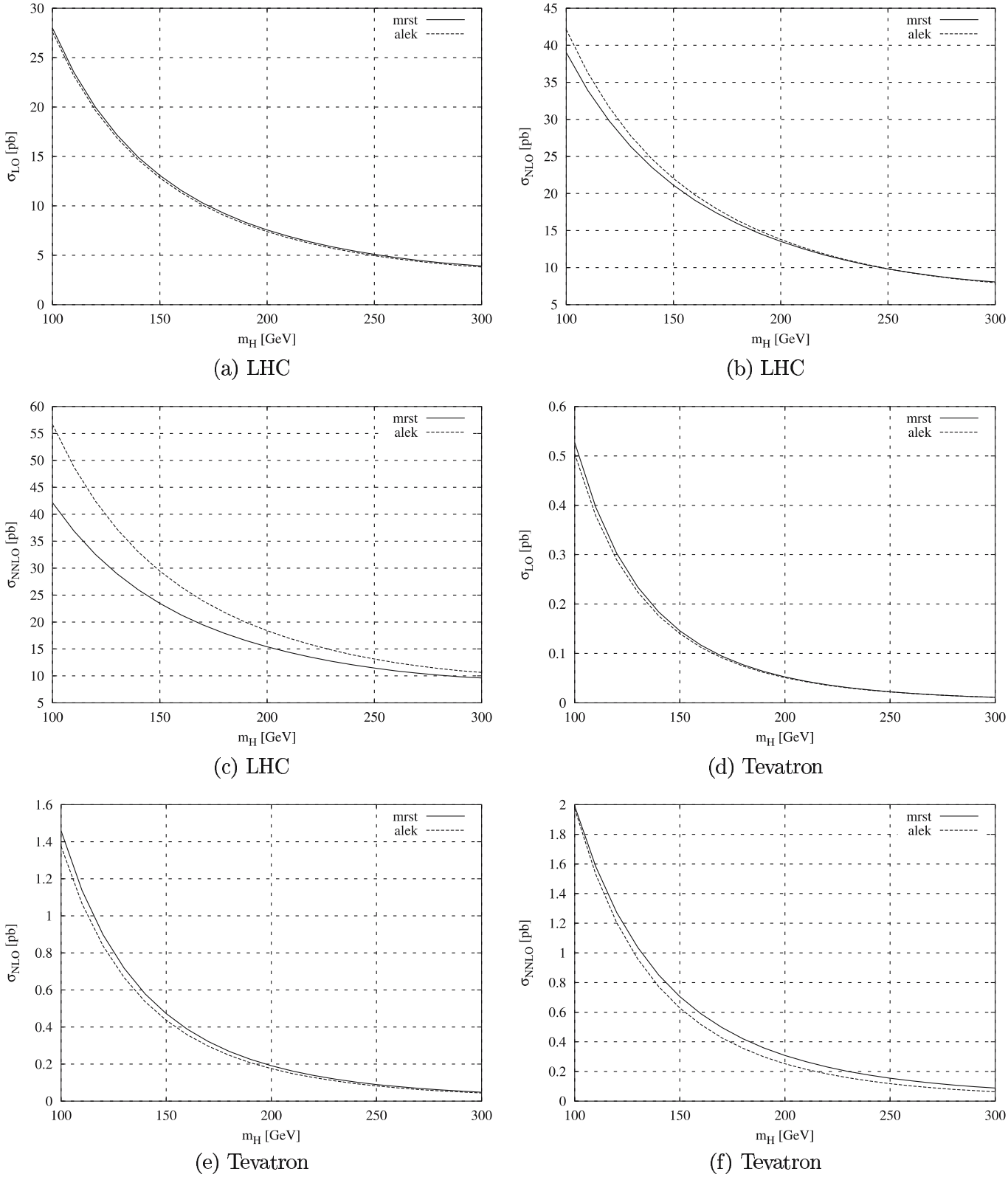

Fig. 6. Cross sections for the scalar Higgs production at the LHC and Tevatron with $\mu_{\rm R}^2 = (1/2)\mu_{\rm F}^2$ and $\mu_{\rm F} = 2m_H$

ond solutions include higher order terms in $a_{\rm s}$ and can be identified only in the non-singlet case. Exact approaches also include an exact solution of the renormalization group equation for the β-function, which embodies the effects of the coefficients β_0, β_1 and β_2 to higher order in $a_{\rm s}$. The term "exact" is, however, a misnomer since the accuracy of the solution is limited to the knowledge of the first three contributions to the expansion in the beta function and in

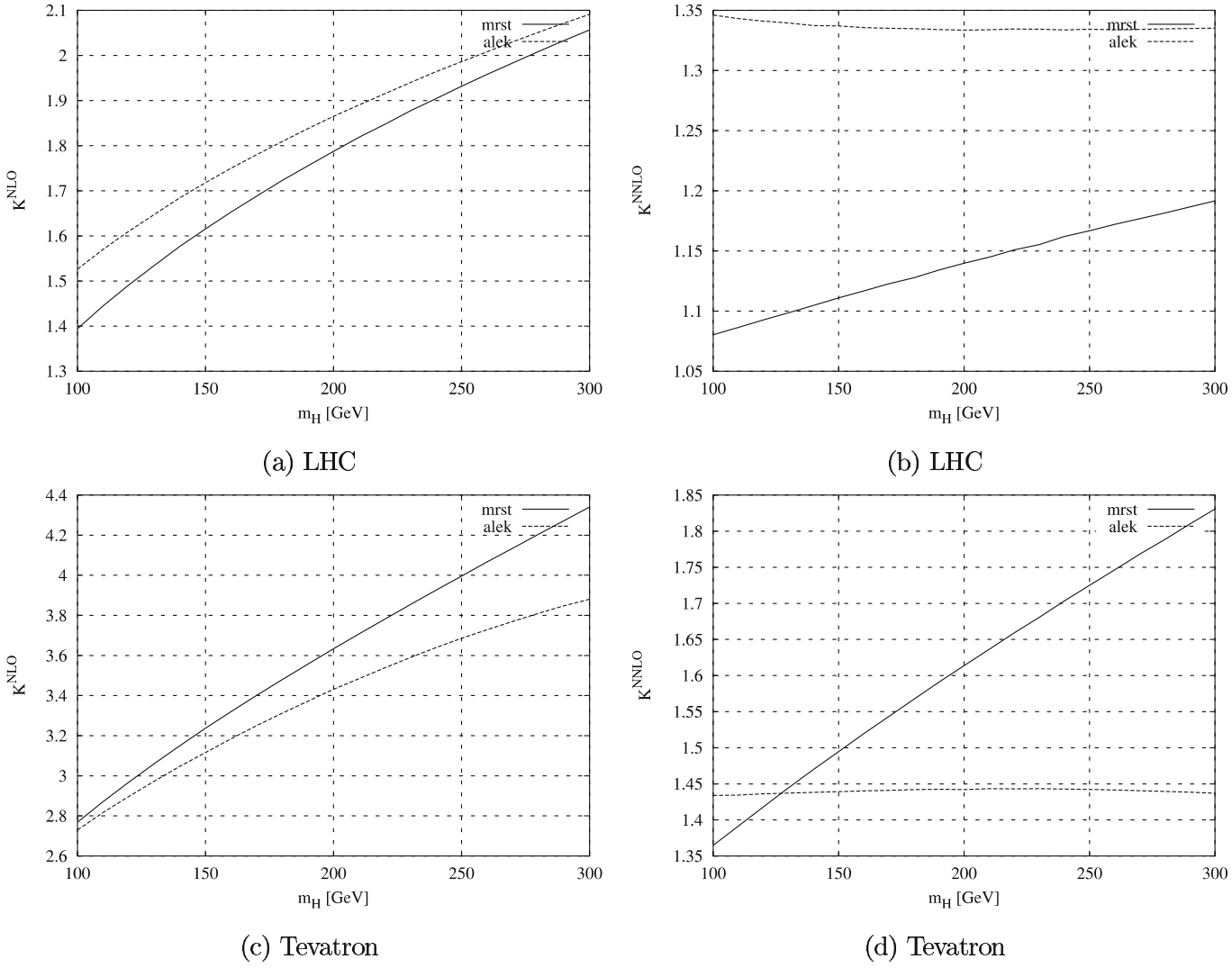

Fig. 7. K-factors for the scalar Higgs at NNLO/NLO and NLO/LO with $\mu_{\rm R}^2 = (1/2)\mu_{\rm F}^2$ and $\mu_{\rm F} = 2m_H$

the kernels. It can be shown both for exact and for the truncated solutions that solving the equations by an ansatz in x-space is completely equivalent to searching for the solution in moment space, since in moment space the recursion relations can be solved exactly [15].

A numerical comparison of our approach with that of [18] has been presented in [15] where it is shown that at LO and NLO there is excellent agreement, while at NNLO there are discrepancies of a few percent (mainly in the singlet case, and at very small and large x values). For a more detailed discussion we refer the reader to Sect. 11 of [15].

4 Renormalization scale dependence

For a better determination of the dependence of the perturbative cross section on the scales of a certain process it is important to keep these scales independent and study the behavior of the corresponding hadronic cross section under their variation. In our case the two relevant scales are the factorization scale $\mu_{\rm F}$ and the renormalization scale $\mu_{\rm R}$, which can both be included in the evolution by a rearrangement of the evolution kernels up to NNLO.

The study of the dependence of the solution upon the various scales is then performed in great generality and includes also the logarithmic contributions $\log(\mu_{\rm F}/\mu_{\rm R})$ coming from the hard scatterings given in [2], where, however, only the specific point $\mu_{\rm F} = \mu_{\rm R} = m_H$ was considered. The separation of the scales should then appear not only in the hard scatterings but also in the evolution equations. This issue has been addressed in [18] and can be reconsidered also from x-space [15] using the x-space logarithmic ansatz (11).

The scale dependence of the parton distribution functions is then expressed by a generalized DGLAP equation

$$\frac{\partial}{\partial \ln \mu_{\rm F}^2} f_i\left(x, \mu_{\rm F}^2, \mu_{\rm R}^2\right) = P_{ij}\left(x, \mu_{\rm F}^2, \mu_{\rm R}^2\right) \otimes f_j\left(x, \mu_{\rm F}^2, \mu_{\rm R}^2\right), \tag{12}$$

where $\mu_{\rm F}$ is now a generic factorization scale.

Table 1. Values of the cross sections and K-factors for the scalar Higgs production at the LHC as a function of $\sqrt{S}$ with $\mu_{\rm F} = m_H$, with $\mu_{\rm F}^2 = \mu_{\rm R}^2$ and $m_H = 114$ GeV for Alekhin, with errors

$\sqrt{S}$	$\sigma_{\rm LO}$	$\sigma_{\rm NLO}$	$\sigma_{\rm NNLO}$	$K^{\rm NLO}$	$K^{\rm NNLO}$
2.0	0.3981 ± 0.0013	0.861 ± 0.002	1.090 ± 0.003	2.162 ± 0.009	1.266 ± 0.005
2.5	0.712 ± 0.003	1.499 ± 0.004	1.895 ± 0.006	2.106 ± 0.011	1.264 ± 0.005
3.0	1.111 ± 0.006	2.291 ± 0.007	2.888 ± 0.011	2.062 ± 0.013	1.261 ± 0.006
3.5	1.589 ± 0.011	3.222 ± 0.010	4.049 ± 0.017	2.028 ± 0.015	1.257 ± 0.006
4.0	2.141 ± 0.017	4.279 ± 0.015	5.36 ± 0.02	1.999 ± 0.018	1.253 ± 0.007
4.5	2.76 ± 0.03	5.45 ± 0.02	6.81 ± 0.04	1.974 ± 0.020	1.249 ± 0.008
5.0	3.45 ± 0.04	6.73 ± 0.03	8.38 ± 0.05	1.95 ± 0.02	1.245 ± 0.009
5.5	4.19 ± 0.05	8.10 ± 0.04	10.06 ± 0.07	1.93 ± 0.02	1.241 ± 0.010
6.0	5.00 ± 0.06	9.57 ± 0.05	11.85 ± 0.09	1.92 ± 0.03	1.238 ± 0.012
6.5	5.85 ± 0.08	11.12 ± 0.07	13.73 ± 0.12	1.90 ± 0.03	1.235 ± 0.013
7.0	6.76 ± 0.10	12.74 ± 0.09	15.70 ± 0.15	1.89 ± 0.03	1.232 ± 0.015
7.5	7.71 ± 0.13	14.44 ± 0.11	17.75 ± 0.19	1.87 ± 0.03	1.229 ± 0.016
8.0	8.71 ± 0.16	16.21 ± 0.14	19.9 ± 0.2	1.86 ± 0.04	1.226 ± 0.018
8.5	9.75 ± 0.19	18.04 ± 0.18	22.1 ± 0.3	1.85 ± 0.04	1.224 ± 0.020
9.0	10.8 ± 0.2	19.9 ± 0.2	24.4 ± 0.3	1.84 ± 0.04	1.22 ± 0.02
9.5	12.0 ± 0.3	21.9 ± 0.3	26.7 ± 0.4	1.83 ± 0.04	1.22 ± 0.02
10.0	13.1 ± 0.3	23.9 ± 0.3	29.1 ± 0.5	1.82 ± 0.05	1.22 ± 0.03
10.5	14.3 ± 0.4	25.9 ± 0.4	31.5 ± 0.6	1.81 ± 0.05	1.21 ± 0.03
11.0	15.6 ± 0.4	28.1 ± 0.4	34.0 ± 0.7	1.80 ± 0.06	1.21 ± 0.03
11.5	16.8 ± 0.5	30.2 ± 0.5	36.6 ± 0.8	1.80 ± 0.06	1.21 ± 0.03
12.0	18.1 ± 0.5	32.4 ± 0.6	39.2 ± 0.9	1.79 ± 0.06	1.21 ± 0.04
12.5	19.4 ± 0.6	34.6 ± 0.7	41.8 ± 1.1	1.78 ± 0.07	1.21 ± 0.04
13.0	20.8 ± 0.7	36.9 ± 0.8	44.5 ± 1.2	1.77 ± 0.07	1.21 ± 0.04
13.5	22.2 ± 0.8	39.2 ± 0.9	47.2 ± 1.4	1.77 ± 0.07	1.20 ± 0.04
14.0	23.6 ± 0.9	41.6 ± 1.0	50.0 ± 1.5	1.76 ± 0.08	1.20 ± 0.05

Generally speaking, both the kernels and the PDF's have a dependence on the scales $\mu_{\rm F}$ and $\mu_{\rm R}$, and formally, a comparison between these scales is always possible up to a fixed order by using the renormalization group equations for the running coupling $\alpha_{\rm s}$.

The renormalization scale dependence of the ansatz (11) that solves (12) is obtained quite straightforwardly by a Taylor expansion of the running coupling $\alpha_{\rm s}(\mu_{\rm F}^2)$ in terms of $\alpha_{\rm s}(\mu_{\rm R}^2)$ [15]

$$\alpha_{\rm s}\left(\mu_{\rm F}^2\right) = \alpha_{\rm s}\left(\mu_{\rm R}^2\right) - \left[\frac{\alpha_{\rm s}^2\left(\mu_{\rm R}^2\right)}{4\pi} + \frac{\alpha_{\rm s}^3\left(\mu_{\rm R}^2\right)}{(4\pi)^2}\left(-\beta_0^2 L^2 + \beta_1 L\right)\right] \tag{13}$$

where the $\mu_{\rm F}^2$ dependence is included in the factor $L = \ln(\mu_{\rm F}^2/\mu_{\rm R}^2)$, and the coefficients of the β-function (the β_i) are listed here [19–21]:

$$\begin{aligned}
\beta_0 &= \frac{11}{3}N_C - \frac{4}{3}T_f,\\
\beta_1 &= \frac{34}{3}N_C^2 - \frac{10}{3}N_C n_f - 2C_{\rm F} n_f,\\
\beta_2 &= \frac{2857}{54}N_C^3 + 2C_{\rm F}^2 T_f - \frac{205}{9}C_{\rm F} N_C T_f - \frac{1415}{27}N_C^2 T_f\\
&\quad + \frac{44}{9}C_{\rm F} T_f^2 + \frac{158}{27}N_C T_f^2\,.
\end{aligned} \tag{14}$$

As usual we have set

$$N_C = 3, \quad C_{\rm F} = \frac{N_C^2 - 1}{2N_C} = \frac{4}{3}, \quad T_f = T_{\rm R} n_f = \frac{1}{2}n_f\,, \tag{15}$$

where N_C is the number of colors and n_f is the number of active flavors. This number is varied as we step into a region characterized by an evolution scale μ larger than a specific quark mass ($\mu \geq m_{\rm q}$). Also the NNLO matching conditions across flavor thresholds [22, 23] are implemented.

Since the perturbative expansion of (10) contains powers of $\alpha_s(\mu_{\rm F}^2)$ which can be related to the value of $\alpha_{\rm s}(\mu_{\rm R}^2)$ by (13), from

$$P_{ij}^{\rm NNLO}(x, \mu_{\rm F}^2) = \sum_{k=0}^{2}\left(\frac{\alpha_{\rm s}(\mu_{\rm F}^2)}{4\pi}\right)^{k+1} P_{ij}^{(k)}(x)\,, \tag{16}$$

substituting (13) into (16), we obtain the corresponding expression of the kernels organized in powers of $\alpha_s(\mu_{\rm R}^2)$ up to NNLO, and it reads [18]

$$\begin{aligned}
P_{ij}(x, \mu_{\rm F}^2, \mu_{\rm R}^2) &= \frac{\alpha_{\rm s}(\mu_{\rm R}^2)}{4\pi}P_{ij}^{(0)}(x)\\
&\quad + \frac{\alpha_{\rm s}^2(\mu_{\rm R}^2)}{(4\pi)^2}\left(P_{ij}^{(1)}(x) - \beta_0 P_{ij}^{(0)}(x) L\right)\\
&\quad + \frac{\alpha_{\rm s}^3(\mu_{\rm R}^2)}{(4\pi)^3}\\
&\quad \times \left[P_{ij}^{(2)}(x) - 2\beta_0 L P_{ij}^{(1)}(x) - \left(\beta_1 L - \beta_0^2 L^2\right) P_{ij}^{(0)}(x)\right]\,.
\end{aligned} \tag{17}$$

The implementation of the method in x-space is quite straightforward and allows us to perform a separate study of the predictions in terms of $\mu_{\rm F}$ and $\mu_{\rm R}$.

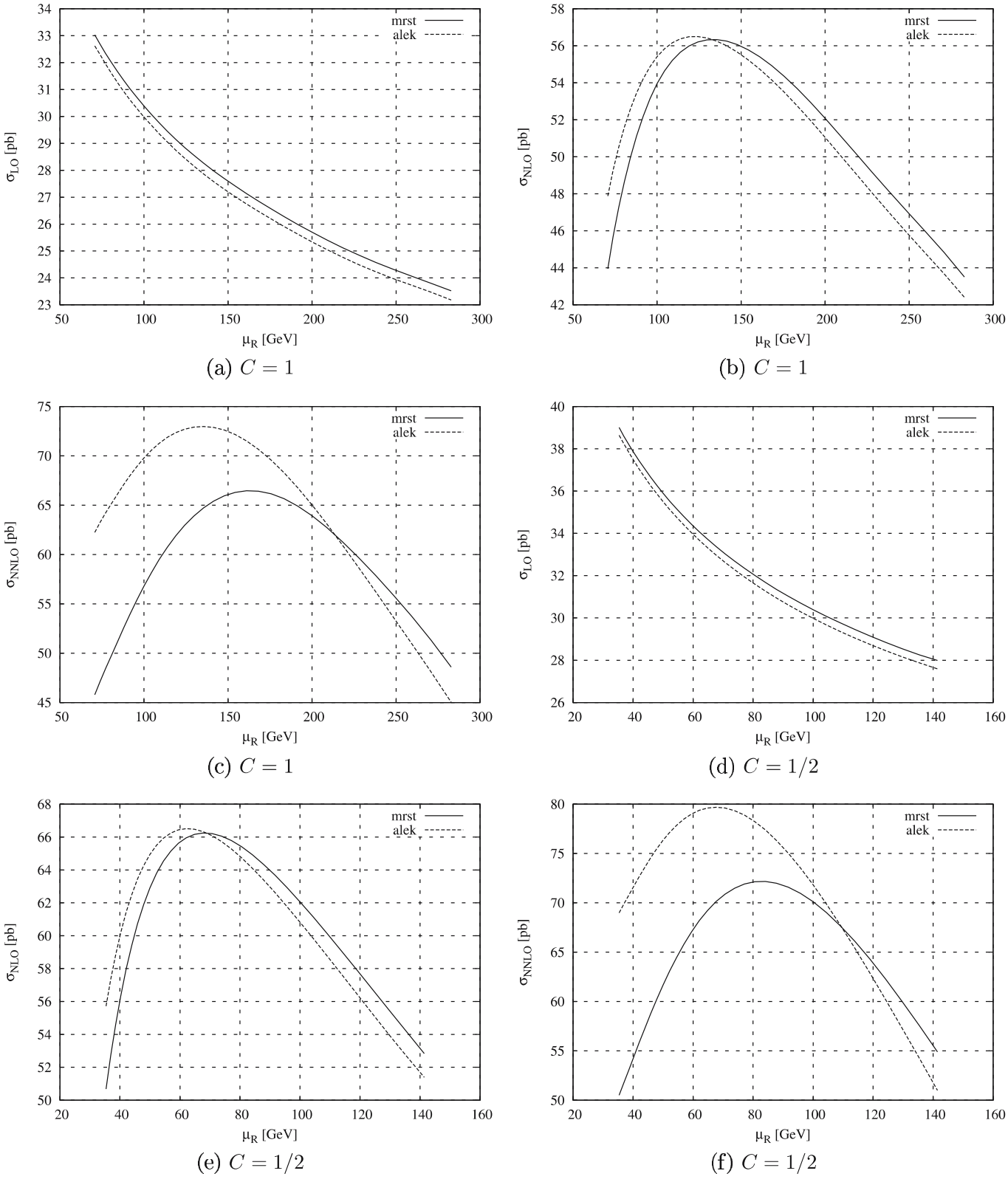

(a) $C = 1$ (b) $C = 1$

(c) $C = 1$ (d) $C = 1/2$

(e) $C = 1/2$ (f) $C = 1/2$

Fig. 8. Cross sections for the scalar Higgs production at the LHC as a function of μ_R, with $\mu_F = Cm_H$ and $m_H = 100\,\text{GeV}$

5 Numerical results

The use of the NNLO evolution of the parton distributions together with the results of [2] allows us to provide accurate predictions for the total cross section for Higgs production. Here we summarize and discuss our numerical results.

We use as initial conditions at low scales the sets of distributions given by MRST [24] and Alekhin [25]. Our final

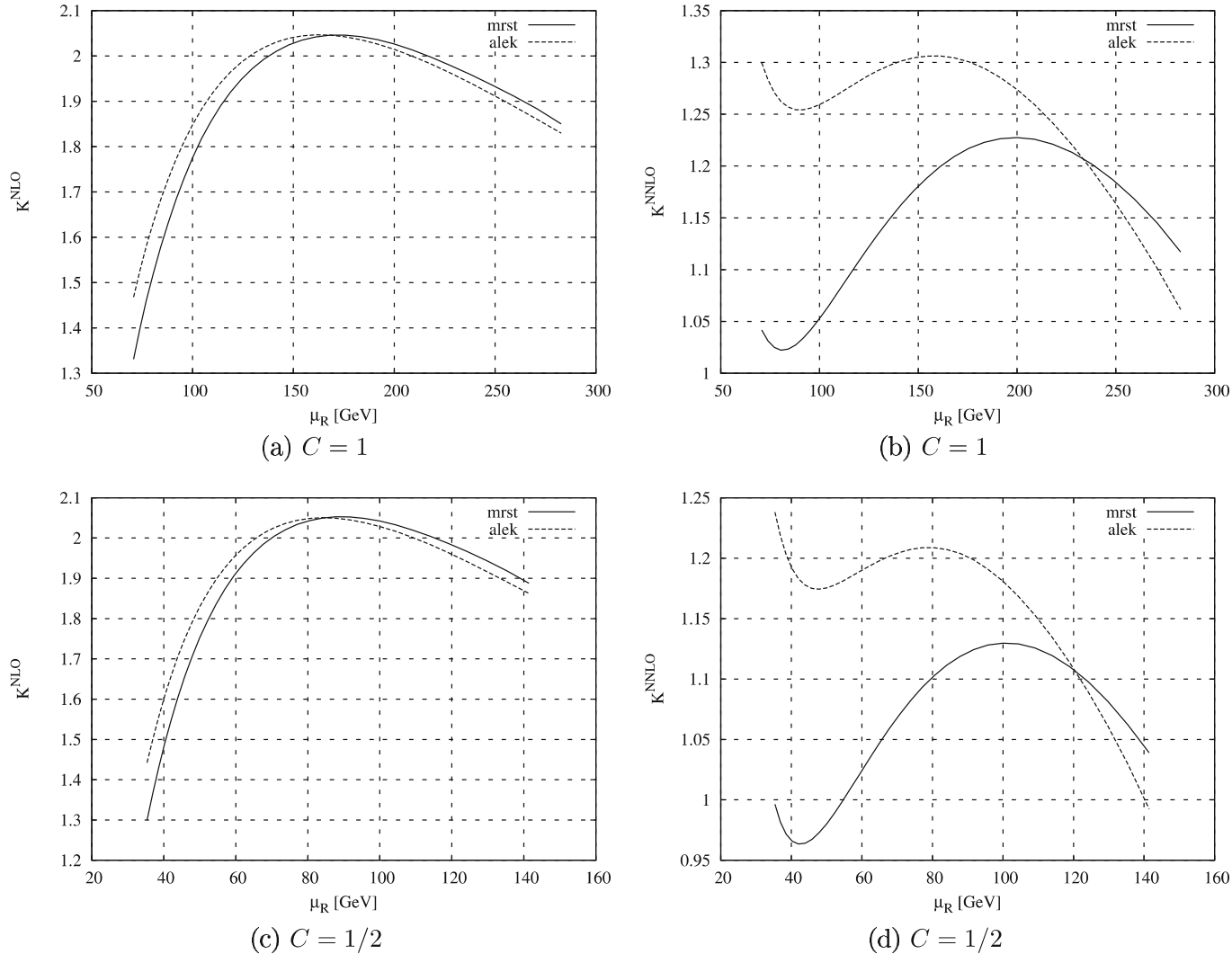

Fig. 9. K-factors for the scalar Higgs production at the LHC, NNLO/NLO and NLO/LO as a function of $\mu_{\rm R}$, with $\mu_{\rm F} = Cm_H$ and $m_H = 100$ GeV

plots refer to center-of-mass energies which are reachable at the LHC, with 14 TeV being the largest one achievable in a not so distant future, and at the Tevatron, where we have selected the corresponding value as 2 TeV. We have also taken the Higgs mass m_H as a parameter in the prediction, with an interval of variability which goes from a light to a heavy Higgs (100 GeV to 300 GeV). Therefore $\mu_{\rm F}$, $\mu_{\rm R}$ and m_H are studied choosing various combinations of their possible values in the determination of total cross sections at leading ($\sigma_{\rm LO}$), next-to-leading ($\sigma_{\rm NLO}$), and next-to-next-to-leading order ($\sigma_{\rm NNLO}$). We present both standard two-dimensional plots and also some three-dimensional plots in order to characterize in detail the structure of the region of stability of the perturbative expansion. We have also evaluated the K-factors for the total Higgs cross section at NLO, defined by

$$K^{\rm NLO} = \frac{\sigma_{\rm NLO}}{\sigma_{\rm LO}}, \tag{18}$$

and at NNLO,

$$K^{\rm NNLO} = \frac{\sigma_{\rm NNLO}}{\sigma_{\rm NLO}}. \tag{19}$$

The study of the K-factors has been performed first by keeping the three scales equal ($\mu_{\rm F} = \mu_{\rm R} = m_H$) and then letting them vary around the typical value m_H. A second set of studies has been performed by taking typical values of m_H and varying the value of the renormalization scale.

5.1 The errors on the cross sections

We present in Figs. 3 and 4 the LO, NLO and NNLO results for the total Higgs cross sections at the LHC ($\sqrt{S} = 14$ TeV) and at the Tevatron ($\sqrt{S} = 2$ TeV), with the corresponding errors, by setting the condition $\mu_{\rm R} = \mu_{\rm F}$. We have chosen to compute these only for two figures, as an illustration of the size of the errors on the parton distribution functions compared to the best fits, since these are smaller than the variation induced when moving from one

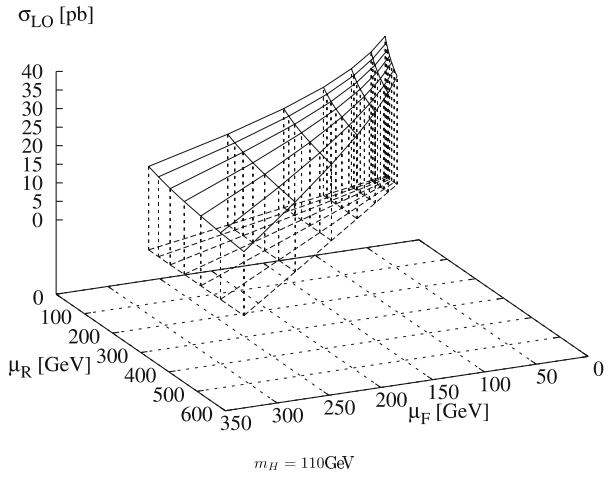

Fig. 10. Three-dimensional graphs for the LO cross sections for the scalar Higgs production at the LHC, as a function of μ_{R} and with μ_{F} with a fixed value of m_H

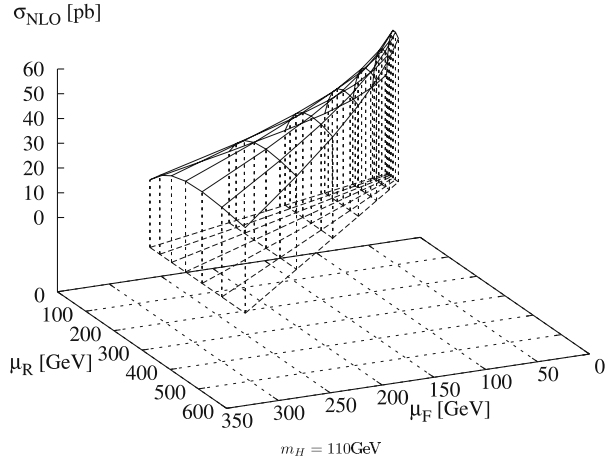

Fig. 11. Three-dimensional graphs for the NLO cross sections for the scalar Higgs production at the LHC, as a function of μ_{R} and with μ_{F} with a fixed value of m_H

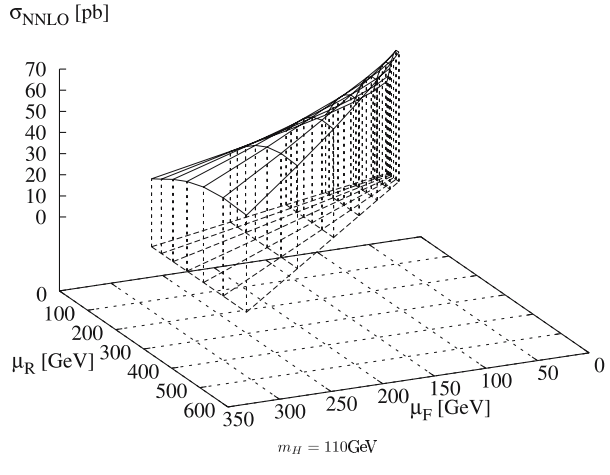

Fig. 12. Three-dimensional graphs for the NNLO cross sections for the scalar Higgs production at the LHC, as a function of μ_{R} and with μ_{F} with a fixed value of m_H

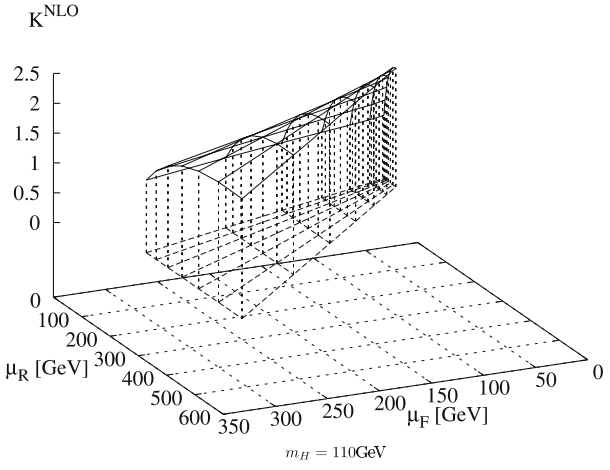

Fig. 13. Three-dimensional graphs for the K-factor $\sigma_{\mathrm{NLO}}/\sigma_{\mathrm{LO}}$ for the scalar Higgs production at the LHC, as a function of μ_{R} and μ_{F} and at a fixed value of m_H

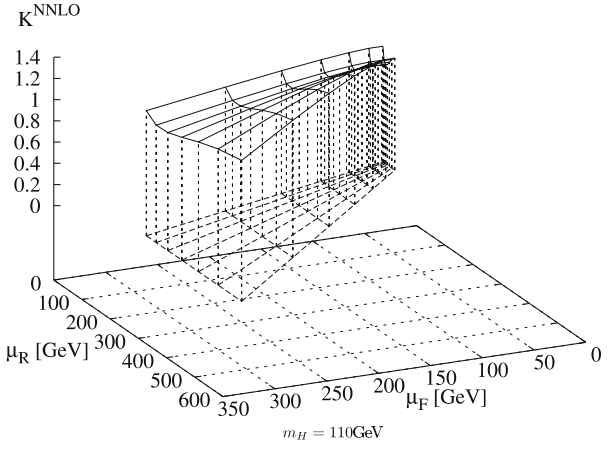

Fig. 14. Three-dimensional graphs for the K-factor $\sigma_{\mathrm{NNLO}}/\sigma_{\mathrm{NLO}}$ for the scalar Higgs production at the LHC, as a function of μ_{R} and μ_{F} and at a fixed value of m_H

perturbative order to the next. The numerical determination of the errors is computationally very intensive and has been performed on a cluster.

In the figures on the left the cross sections obtained using MRST input are represented by a solid line, and the ones obtained using Alekhin's input by a dashed line. In the figures on the right we present a plot of the difference between the values of the MRST cross sections and Alekhin's cross sections for each perturbative order, with the respective errors. The calculation of the error bands has been done following the usual theory of the linear propagation of the errors. Starting from the errors on the PDFs known in the literature [25, 26], we have generated different sets of cross sections. Then, the error on the cross section has been calculated using the formula

$$\Delta\sigma = \frac{1}{2}\sqrt{\sum_{k=1}^{N}\left[\sigma_{2k-1}-\sigma_{2k}\right]^2}\,, \tag{20}$$

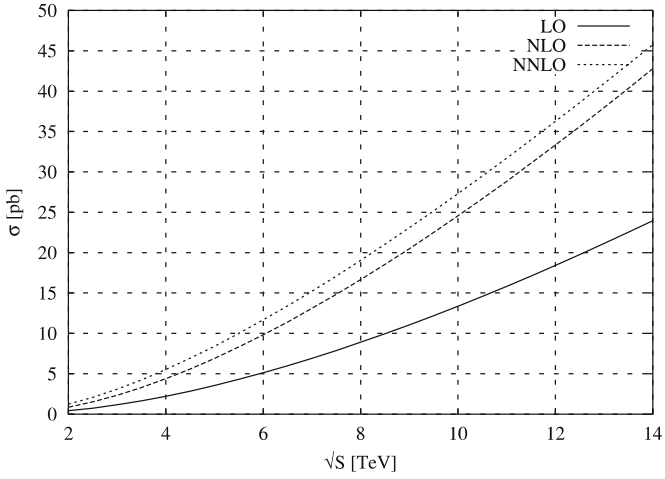

(a) $C = 1,\ k = 1$

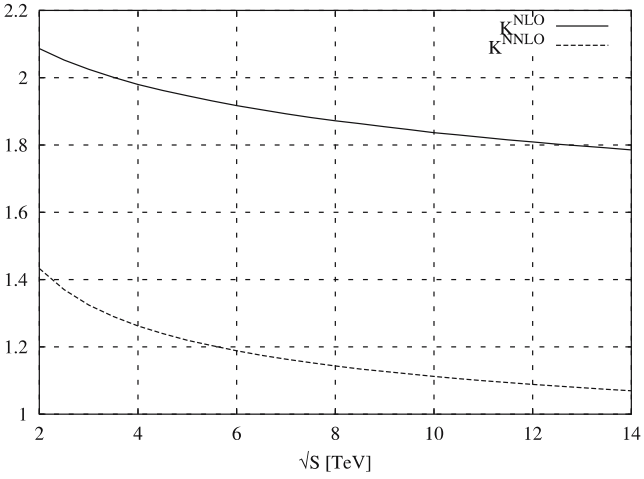

(b) $C = 1,\ k = 1$

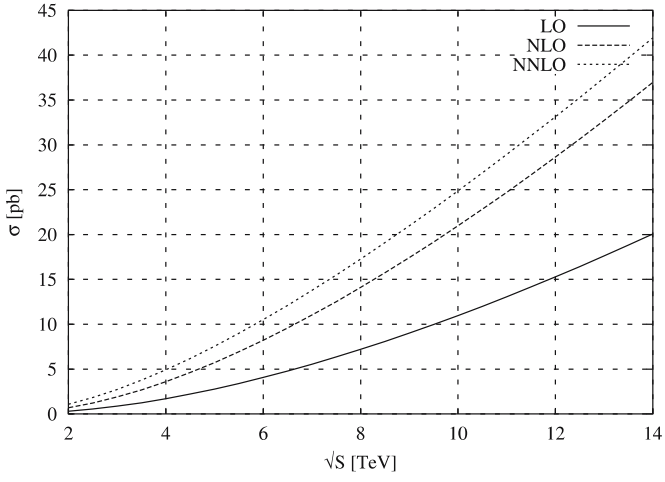

(c) $C = 2,\ k = 1$

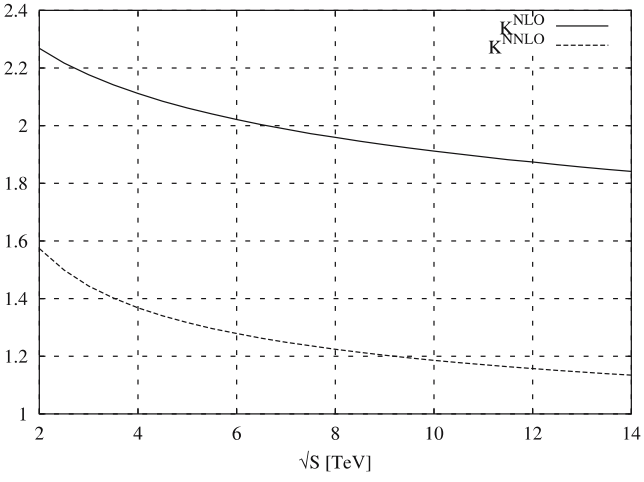

(d) $C = 2,\ k = 1$

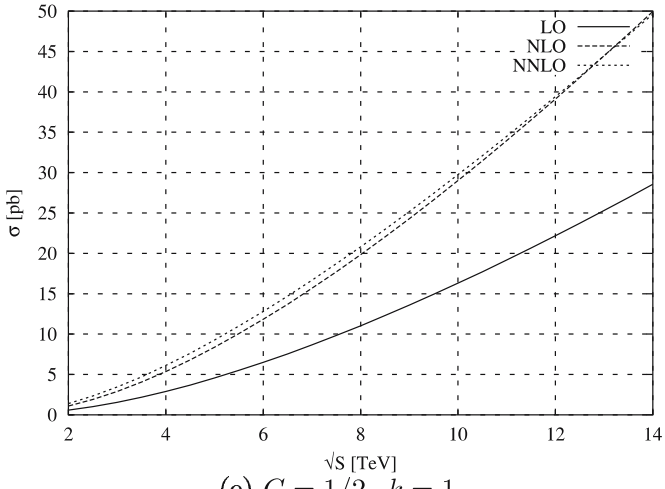

(e) $C = 1/2,\ k = 1$

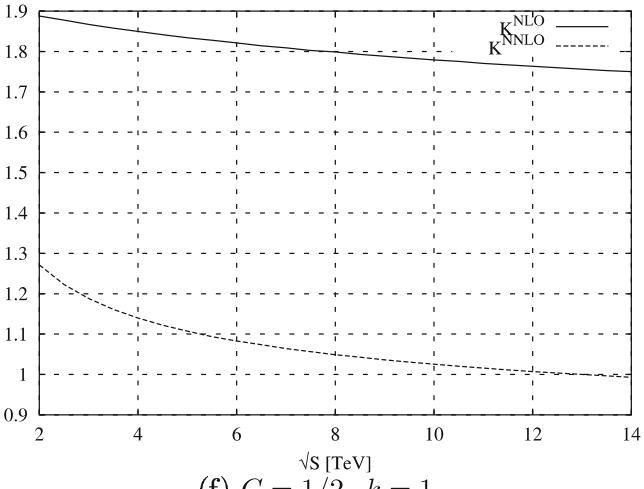

(f) $C = 1/2,\ k = 1$

Fig. 15. Cross sections and K-factors for the scalar Higgs production at the LHC as a function of $\sqrt{S}$ with $\mu_{\mathrm{F}} = Cm_H$, with $\mu_{\mathrm{F}}^2 = k\mu_{\mathrm{R}}^2$ and $m_H = 114\,\mathrm{GeV}$. MRST inputs have been used

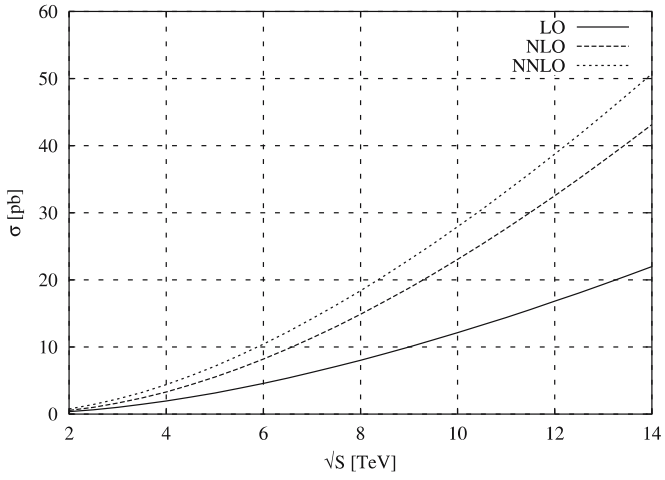

(a) $C = 1,\ k = 2$

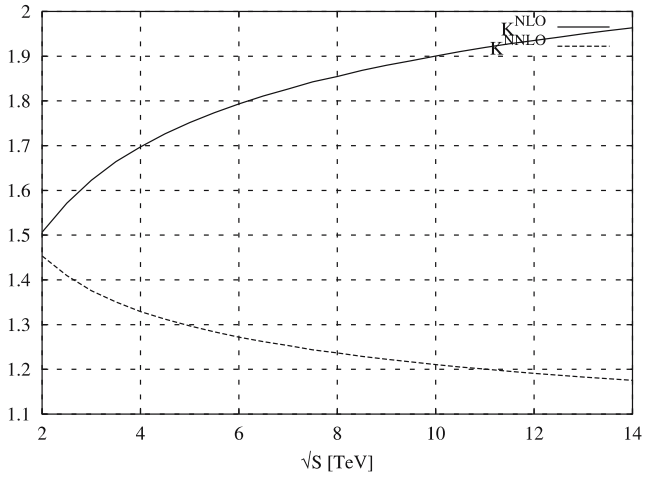

(b) $C = 1,\ k = 2$

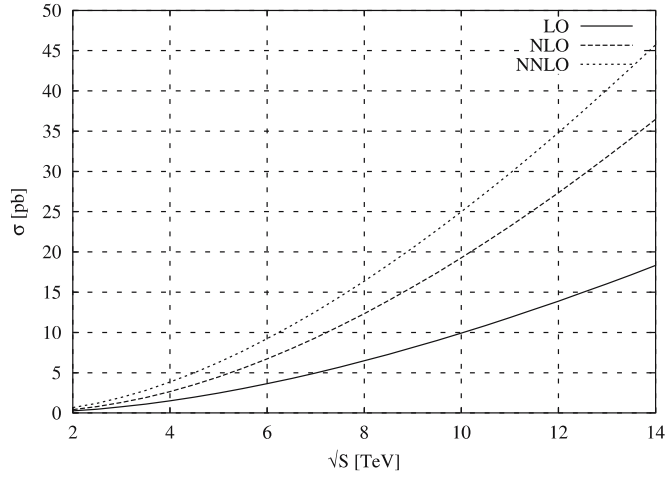

(c) $C = 2,\ k = 2$

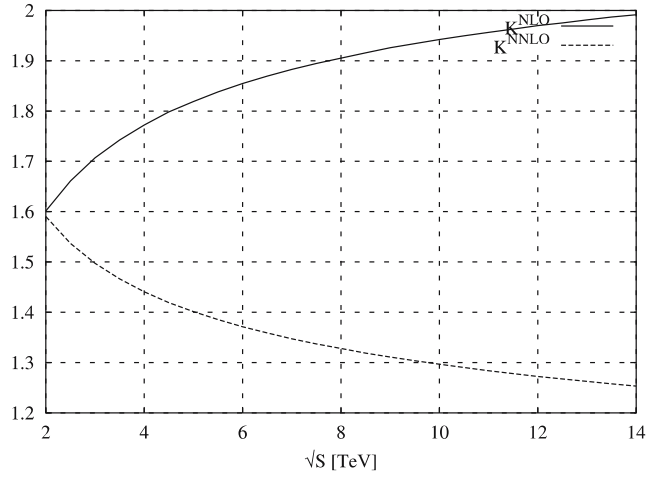

(d) $C = 2,\ k = 2$

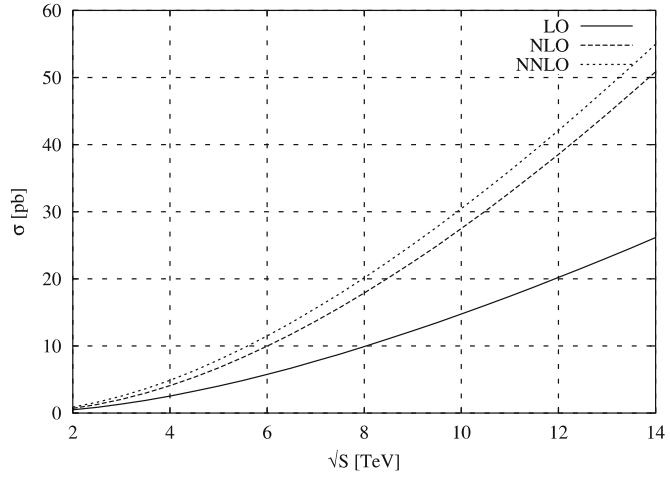

(e) $C = 1/2,\ k = 2$

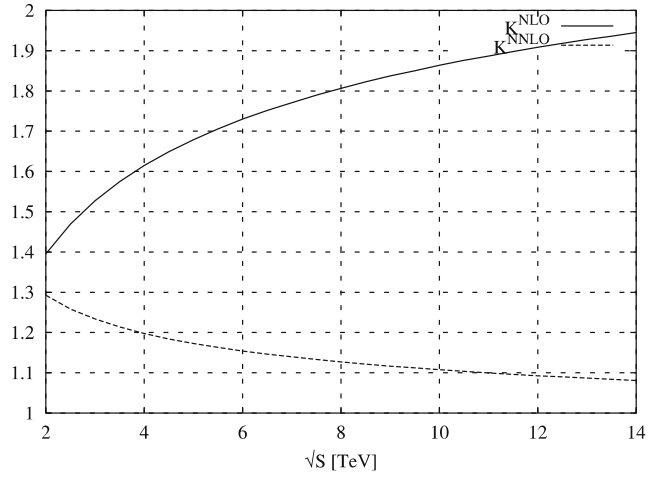

(f) $C = 1/2,\ k = 2$

Fig. 16. Cross sections and K-factors for the scalar Higgs production at the LHC as a function of $\sqrt{S}$ with $\mu_{\rm F} = Cm_H$, with $\mu_{\rm F}^2 = k\mu_{\rm R}^2$ and $m_H = 114\,\text{GeV}$. MRST inputs have been used

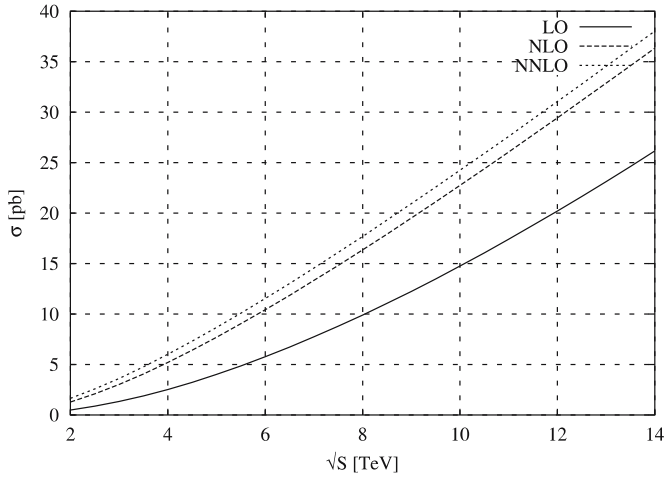

(a) $C = 1,\ k = 1/2$

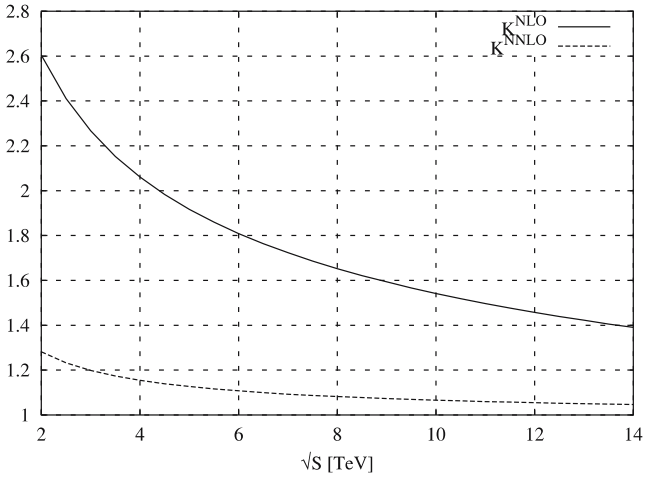

(b) $C = 1,\ k = 1/2$

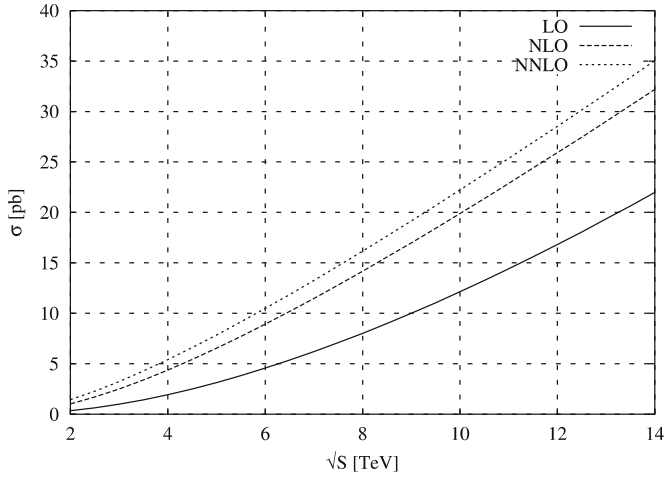

(c) $C = 2,\ k = 1/2$

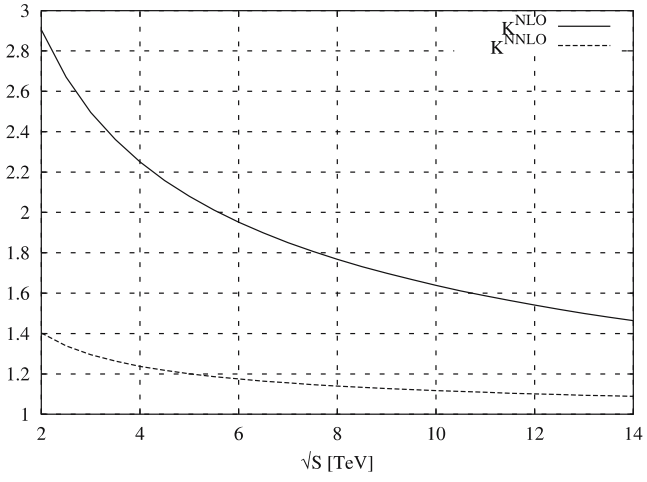

(d) $C = 2,\ k = 1/2$

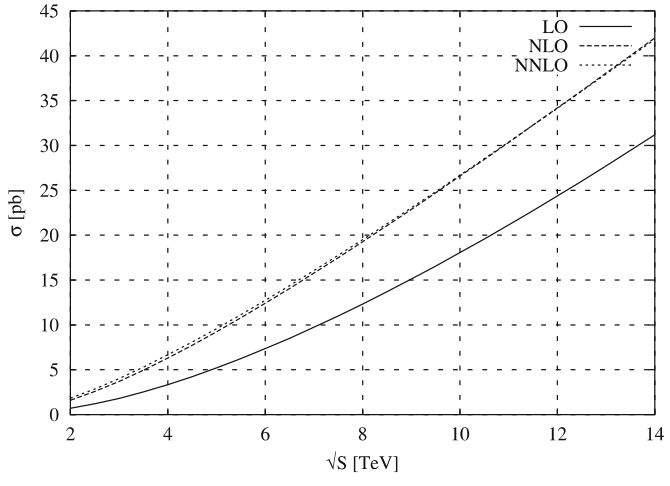

(e) $C = 1/2,\ k = 1/2$

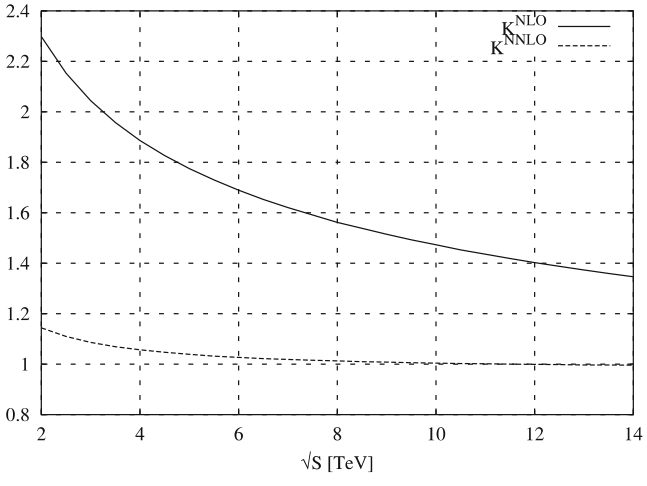

(f) $C = 1/2,\ k = 1/2$

Fig. 17. Cross sections and K-factors for the scalar Higgs production at the LHC as a function of $\sqrt{S}$ with $\mu_{\mathrm{F}} = Cm_H$, with $\mu_{\mathrm{F}}^2 = k\mu_{\mathrm{R}}^2$ and $m_H = 114\,\mathrm{GeV}$. MRST inputs have been used

Table 2. Values of the cross sections and K-factors for the scalar Higgs production at the LHC as a function of $\sqrt{S}$ with $\mu_{\rm F} = m_H$, with $\mu_{\rm F}^2 = \mu_{\rm R}^2$ and $m_H = 114\,\text{GeV}$. MRST inputs have been used

$\sqrt{S}$	$\sigma_{\rm LO}$	$\sigma_{\rm NLO}$	$\sigma_{\rm NNLO}$	$K^{\rm NLO}$	$K^{\rm NNLO}$
2.0	0.4155	0.8670	1.242	2.087	1.433
2.5	0.7410	1.521	2.084	2.053	1.370
3.0	1.153	2.335	3.093	2.025	1.325
3.5	1.645	3.292	4.248	2.001	1.290
4.0	2.212	4.380	5.529	1.980	1.262
4.5	2.847	5.587	6.924	1.962	1.239
5.0	3.547	6.903	8.419	1.946	1.220
5.5	4.308	8.318	10.01	1.931	1.203
6.0	5.125	9.826	11.68	1.917	1.189
6.5	5.995	11.42	13.42	1.905	1.175
7.0	6.916	13.09	15.23	1.893	1.163
7.5	7.885	14.84	17.11	1.882	1.153
8.0	8.899	16.66	19.05	1.872	1.143
8.5	9.956	18.55	21.04	1.863	1.134
9.0	11.05	20.49	23.09	1.854	1.127
9.5	12.19	22.50	25.18	1.846	1.119
10.0	13.37	24.56	27.31	1.837	1.112
10.5	14.58	26.68	29.49	1.830	1.105
11.0	15.83	28.85	31.71	1.822	1.099
11.5	17.11	31.06	33.97	1.815	1.094
12.0	18.42	33.32	36.26	1.809	1.088
12.5	19.76	35.62	38.59	1.803	1.083
13.0	21.13	37.97	40.95	1.797	1.078
13.5	22.53	40.36	43.33	1.791	1.074
14.0	23.96	42.78	45.75	1.785	1.069

Table 3. Values of the cross sections and K-factors for the scalar Higgs production at the LHC as a function of $\sqrt{S}$ with $\mu_{\rm F} = 2m_H$, with $\mu_{\rm F}^2 = \mu_{\rm R}^2$ and $m_H = 114\,\text{GeV}$. MRST inputs have been used

$\sqrt{S}$	$\sigma_{\rm LO}$	$\sigma_{\rm NLO}$	$\sigma_{\rm NNLO}$	$K^{\rm NLO}$	$K^{\rm NNLO}$
2.0	0.3029	0.6871	1.081	2.268	1.573
2.5	0.5508	1.221	1.830	2.217	1.499
3.0	0.8700	1.893	2.733	2.176	1.444
3.5	1.256	2.690	3.771	2.142	1.402
4.0	1.706	3.602	4.928	2.111	1.368
4.5	2.216	4.619	6.191	2.084	1.340
5.0	2.781	5.733	7.549	2.061	1.317
5.5	3.400	6.937	8.993	2.040	1.296
6.0	4.069	8.225	10.52	2.021	1.279
6.5	4.786	9.590	12.11	2.004	1.263
7.0	5.548	11.03	13.77	1.988	1.248
7.5	6.354	12.53	15.49	1.972	1.236
8.0	7.201	14.11	17.27	1.959	1.224
8.5	8.088	15.74	19.10	1.946	1.213
9.0	9.012	17.43	20.98	1.934	1.204
9.5	9.974	19.17	22.90	1.922	1.195
10.0	10.97	20.97	24.87	1.912	1.186
10.5	12.00	22.82	26.88	1.902	1.178
11.0	13.06	24.71	28.93	1.892	1.171
11.5	14.16	26.65	31.01	1.882	1.164
12.0	15.28	28.63	33.13	1.874	1.157
12.5	16.44	30.65	35.28	1.864	1.151
13.0	17.62	32.71	37.47	1.856	1.146
13.5	18.83	34.81	39.68	1.849	1.140
14.0	20.07	36.95	41.92	1.841	1.135

where σ_k is the kth cross section belonging to a certain set, and N is the number of free parameters, which is 15 for MRST and 17 for Alekhin.

The PDFs with the related error analysis are available at all orders for the Alekhin input but only at NLO for the MRST's input (Fig. 3c and Fig. 4c).

When in Figs. 3, 4, and 5 we plot more than one line for a single set the lower line is the minimal value (best fit minus error) and the upper line is the maximal value (best fit plus error).

The LO cross sections increase by a factor of approximately 100 as we change the energy from 2 TeV, Fig. 4, to 14 TeV, Fig. 3, and sharply decrease as we raise the mass of the Higgs boson. At 14 TeV the range of variation of $\sigma_{\rm LO}$ is between 30 and 5 pb, with the highest value reached for $m_H = 100\,\text{GeV}$.

In the same figures we compare LO, NLO and NNLO cross sections at these two typical energies. It is quite evident that the role of the NLO corrections is to increase by a factor of approximately 2 the LO cross section bringing the interval of variation of $\sigma_{\rm NLO}$ between 60 and 10 pb, for an increasing value of m_H. NNLO corrections at 14 TeV increase these values by an additional 10 per cent compared to the NLO prediction, with a growth which is more pronounced for the set proposed by Alekhin.

Comparing the results computed using the Alekhin and MRST inputs, for the LHC case ($\sqrt{S} = 14\,\text{TeV}$) we observe that at LO (see Fig. 3b) the two sets give results which are compatible within the error bands for $m_H < 150\,\text{GeV}$, while for larger values of m_H we observe only small differences between the two. At NLO, Fig. 3d, where the error analysis is available for both sets, the results are compatible within the error bands for $m_H < 190\,\text{GeV}$, and we have small differences for larger values of the Higgs mass. For the NNLO case, Fig. 3f, we notice that there are sensible differences among the two sets.

By a similar inspection of Fig. 4b, d and f, we notice that at the Tevatron energy of $\sqrt{S} = 2\,\text{TeV}$, the two PDF sets give quite different predictions at all the three orders.

The numerical values of the total cross sections and the K-factors as a function of the center-of-mass energy with the respective errors have also been reported in Table 1, in the case of Alekhin's inputs.

5.2 K-factors

A precise indication on the impact of the NLO/NNLO corrections and the stability of the perturbative expansion comes from a study of the K-factors $K^{\rm NLO}$ and $K^{\rm NNLO}$, defined above. From the plots in Fig. 5 the different behavior of the predictions derived from the two models for the parton distributions is quite evident. At 14 TeV the NLO K-factors from both models are large, as expected, since the LO prediction are strongly scale dependent. The in-

Table 4. Values of the cross sections and K-factors for the scalar Higgs production at the LHC as a function of $\sqrt{S}$ with $\mu_{\rm F} = (1/2)m_H$, with $\mu_{\rm F}^2 = \mu_{\rm R}^2$ and $m_H = 114\,{\rm GeV}$. MRST inputs have been used

$\sqrt{S}$	$\sigma_{\rm LO}$	$\sigma_{\rm NLO}$	$\sigma_{\rm NNLO}$	$K^{\rm NLO}$	$K^{\rm NNLO}$
2.0	0.5817	1.098	1.396	1.888	1.271
2.5	1.014	1.904	2.328	1.878	1.223
3.0	1.551	2.896	3.440	1.867	1.188
3.5	2.182	4.054	4.707	1.858	1.161
4.0	2.899	5.362	6.111	1.850	1.140
4.5	3.695	6.804	7.635	1.841	1.122
5.0	4.563	8.369	9.266	1.834	1.107
5.5	5.498	10.05	10.99	1.828	1.094
6.0	6.496	11.83	12.81	1.821	1.083
6.5	7.552	13.70	14.71	1.814	1.074
7.0	8.662	15.67	16.67	1.809	1.064
7.5	9.824	17.71	18.71	1.803	1.056
8.0	11.03	19.84	20.81	1.799	1.049
8.5	12.29	22.03	22.97	1.793	1.043
9.0	13.59	24.30	25.18	1.788	1.036
9.5	14.93	26.63	27.44	1.784	1.030
10.0	16.31	29.02	29.75	1.779	1.025
10.5	17.72	31.46	32.10	1.775	1.020
11.0	19.18	33.96	34.50	1.771	1.016
11.5	20.66	36.51	36.93	1.767	1.012
12.0	22.18	39.11	39.40	1.763	1.007
12.5	23.73	41.76	41.91	1.760	1.004
13.0	25.31	44.45	44.45	1.756	1.000
13.5	26.92	47.19	47.02	1.753	0.9964
14.0	28.55	49.96	49.62	1.750	0.9932

Table 5. Values of the cross sections and K-factors for the scalar Higgs production at the LHC as a function of $\sqrt{S}$ with $\mu_{\rm F} = m_H$, with $\mu_{\rm F}^2 = 2\mu_{\rm R}^2$ and $m_H = 114\,{\rm GeV}$. MRST inputs have been used

$\sqrt{S}$	$\sigma_{\rm LO}$	$\sigma_{\rm NLO}$	$\sigma_{\rm NNLO}$	$K^{\rm NLO}$	$K^{\rm NNLO}$
2.0	0.3546	0.5343	0.7766	1.507	1.453
2.5	0.6388	1.004	1.415	1.572	1.409
3.0	1.002	1.626	2.237	1.623	1.376
3.5	1.438	2.393	3.232	1.664	1.351
4.0	1.944	3.300	4.387	1.698	1.329
4.5	2.514	4.340	5.694	1.726	1.312
5.0	3.144	5.507	7.142	1.752	1.297
5.5	3.831	6.795	8.724	1.774	1.284
6.0	4.572	8.199	10.43	1.793	1.272
6.5	5.363	9.714	12.26	1.811	1.262
7.0	6.202	11.33	14.20	1.827	1.253
7.5	7.088	13.06	16.24	1.843	1.243
8.0	8.017	14.87	18.39	1.855	1.237
8.5	8.987	16.79	20.63	1.868	1.229
9.0	9.997	18.79	22.97	1.880	1.222
9.5	11.05	20.88	25.40	1.890	1.216
10.0	12.13	23.05	27.91	1.900	1.211
10.5	13.25	25.31	30.50	1.910	1.205
11.0	14.40	27.64	33.18	1.919	1.200
11.5	15.59	30.05	35.92	1.928	1.195
12.0	16.81	32.53	38.74	1.935	1.191
12.5	18.06	35.08	41.63	1.942	1.187
13.0	19.33	37.70	44.59	1.950	1.183
13.5	20.64	40.39	47.61	1.957	1.179
14.0	21.97	43.14	50.70	1.964	1.175

crease of $\sigma_{\rm NLO}$ compared to the LO predictions is between 65 and 90%.

In Fig. 5a one can observe that the impact of the NLO corrections to the LO result predicted by both sets increases for an increasing m_H, with the corrections predicted by Alekhin being the largest ones. The trend of the MRST model in the NNLO versus NLO case, Fig. 5b, is similar, for an increasing Higgs mass ranging from 1.16 to 1.22, while the Alekhin $K^{\rm NNLO}$-factor is approximately constant around a value of 1.21.

The evaluation of the overall impact of this growth on the size of these corrections should, however, also keep into consideration the fact that these corrections are enhanced in a region where the cross section is sharply decreasing (Figs. 3 and 4).

Moving to Tevatron energy we notice that all the K-factors are larger than in the LHC case. For a MRST input we continue to observe a growth of $K^{\rm NLO}$ and $K^{\rm NNLO}$ for an increasing m_H, while for the Alekhin case this trend is slower for $K^{\rm NLO}$, and it is even reversed for $K^{\rm NNLO}$. Unlike the LHC situation, the Alekhin's K-factors are smaller than MRST ones at Tevatron energies.

5.3 Renormalization/factorization scale dependence

Now we turn to an analysis of the dependence of our results on $\mu_{\rm F}$ and $\mu_{\rm R}$. In Fig. 6 we perform this study by computing σ as a function of the Higgs mass for an incoming

Table 6. Values of the cross sections and K-factors for the scalar Higgs production at the LHC as a function of $\sqrt{S}$ with $\mu_{\rm F} = 2m_H$, with $\mu_{\rm F}^2 = 2\mu_{\rm R}^2$ and $m_H = 114\,{\rm GeV}$. MRST inputs have been used

$\sqrt{S}$	$\sigma_{\rm LO}$	$\sigma_{\rm NLO}$	$\sigma_{\rm NNLO}$	$K^{\rm NLO}$	$K^{\rm NNLO}$
2.0	0.2597	0.4159	0.6614	1.601	1.590
2.5	0.4763	0.7912	1.216	1.661	1.537
3.0	0.7574	1.293	1.936	1.707	1.497
3.5	1.100	1.917	2.811	1.743	1.466
4.0	1.501	2.660	3.833	1.772	1.441
4.5	1.956	3.517	4.992	1.798	1.419
5.0	2.464	4.482	6.281	1.819	1.401
5.5	3.021	5.553	7.693	1.838	1.385
6.0	3.625	6.724	9.221	1.855	1.371
6.5	4.275	7.991	10.86	1.869	1.359
7.0	4.967	9.351	12.60	1.883	1.347
7.5	5.700	10.80	14.44	1.895	1.337
8.0	6.472	12.33	16.38	1.905	1.328
8.5	7.282	13.95	18.40	1.916	1.319
9.0	8.127	15.65	20.52	1.926	1.311
9.5	9.008	17.42	22.71	1.934	1.304
10.0	9.923	19.27	24.99	1.942	1.297
10.5	10.87	21.19	27.34	1.949	1.290
11.0	11.85	23.18	29.76	1.956	1.284
11.5	12.86	25.24	32.26	1.963	1.278
12.0	13.89	27.36	34.82	1.970	1.273
12.5	14.96	29.55	37.45	1.975	1.267
13.0	16.05	31.80	40.15	1.981	1.263
13.5	17.17	34.11	42.91	1.987	1.258
14.0	18.32	36.48	45.72	1.991	1.253

Table 7. Values of the cross sections and K-factors for the scalar Higgs production at the LHC as a function of $\sqrt{S}$ with $\mu_{\rm F} = (1/2)m_H$, with $\mu_{\rm F}^2 = 2\mu_{\rm R}^2$ and $m_H = 114\,\text{GeV}$. MRST inputs have been used

$\sqrt{S}$	$\sigma_{\rm LO}$	$\sigma_{\rm NLO}$	$\sigma_{\rm NNLO}$	$K^{\rm NLO}$	$K^{\rm NNLO}$
2.0	0.4899	0.6836	0.8836	1.395	1.293
2.5	0.8642	1.270	1.598	1.470	1.258
3.0	1.333	2.036	2.512	1.527	1.234
3.5	1.890	2.976	3.612	1.575	1.214
4.0	2.526	4.079	4.885	1.615	1.198
4.5	3.237	5.338	6.321	1.649	1.184
5.0	4.016	6.743	7.908	1.679	1.173
5.5	4.858	8.288	9.638	1.706	1.163
6.0	5.761	9.966	11.50	1.730	1.154
6.5	6.719	11.77	13.49	1.752	1.146
7.0	7.730	13.69	15.60	1.771	1.140
7.5	8.790	15.73	17.82	1.790	1.133
8.0	9.898	17.88	20.15	1.806	1.127
8.5	11.05	20.14	22.58	1.823	1.121
9.0	12.24	22.49	25.11	1.837	1.116
9.5	13.48	24.94	27.74	1.850	1.112
10.0	14.75	27.49	30.45	1.864	1.108
10.5	16.06	30.13	33.25	1.876	1.104
11.0	17.41	32.85	36.13	1.887	1.100
11.5	18.79	35.66	39.09	1.898	1.096
12.0	20.20	38.55	42.12	1.908	1.093
12.5	21.64	41.51	45.24	1.918	1.090
13.0	23.11	44.56	48.42	1.928	1.087
13.5	24.62	47.67	51.66	1.936	1.084
14.0	26.15	50.86	54.98	1.945	1.081

Table 8. Values of the cross sections and K-factors for the scalar Higgs production at the LHC as a function of $\sqrt{S}$ with $\mu_{\rm F} = m_H$, with $\mu_{\rm F}^2 = (1/2)\mu_{\rm R}^2$ and $m_H = 114\,\text{GeV}$. MRST inputs have been used

$\sqrt{S}$	$\sigma_{\rm LO}$	$\sigma_{\rm NLO}$	$\sigma_{\rm NNLO}$	$K^{\rm NLO}$	$K^{\rm NNLO}$
2.0	0.4899	1.276	1.635	2.605	1.281
2.5	0.8641	2.083	2.567	2.411	1.232
3.0	1.333	3.022	3.622	2.267	1.199
3.5	1.890	4.069	4.775	2.153	1.174
4.0	2.526	5.206	6.009	2.061	1.154
4.5	3.237	6.419	7.312	1.983	1.139
5.0	4.016	7.698	8.673	1.917	1.127
5.5	4.858	9.034	10.08	1.860	1.116
6.0	5.761	10.42	11.54	1.809	1.107
6.5	6.719	11.85	13.03	1.764	1.100
7.0	7.730	13.32	14.55	1.723	1.092
7.5	8.790	14.82	16.11	1.686	1.087
8.0	9.898	16.35	17.69	1.652	1.082
8.5	11.05	17.91	19.30	1.621	1.078
9.0	12.24	19.50	20.93	1.593	1.073
9.5	13.48	21.11	22.57	1.566	1.069
10.0	14.75	22.74	24.24	1.542	1.066
10.5	16.06	24.39	25.92	1.519	1.063
11.0	17.41	26.06	27.61	1.497	1.059
11.5	18.79	27.74	29.32	1.476	1.057
12.0	20.20	29.44	31.05	1.457	1.055
12.5	21.64	31.15	32.78	1.439	1.052
13.0	23.11	32.87	34.53	1.422	1.051
13.5	24.62	34.60	36.28	1.405	1.049
14.0	26.15	36.35	38.04	1.390	1.046

energy of 2 and 14 TeV and choose

$$\mu_{\rm R}^2 = \frac{1}{2}\mu_{\rm F}^2 \quad \mu_{\rm F} = 2m_H\,. \tag{21}$$

We have seen that for a typical Higgs mass around 100 GeV and 14 TeV of energy (for $m_H = \mu_{\rm F} = \mu_{\rm R}$) the cross section doubles when we move from LO to NNLO, and a similar trend is also apparent if we fix the relations among the scales as in (21). In this case, however, the impact of the NLO and NNLO corrections is smaller, a trend which is apparently uniform over the whole range of the Higgs mass explored. For $m_H = 100\,\text{GeV}$ the scalar cross section $\sigma_{\rm NNLO}$ is around 58 pb for coincident scales, while a different choice, such as (21), lowers it to approximately 45 pb. At Tevatron energies the variations of the cross section with the changes of the various scales are also sizeable. In this case for $m_H = 100\,\text{GeV}$ the LO, NLO and NNLO predictions (0.6, 1.2 and 1.6 pb respectively) change approximately by 10%–20% if we include variations of the other scales as well. A parallel view of this trend comes from the study of the dependence of the K-factors. This study is presented in Fig. 7. The interval of variation of the K-factors is substantially the same as for coincident scales, though the trends of the two models [24] and [25] are structurally quite different at NLO and at NNLO, with several cross-overs among the corresponding curves taking place for m_H around 200 GeV. Another important point is that the values of $K^{\rm NNLO}$ are, of course smaller than $K^{\rm NLO}$ over all the regions explored, signaling an overall stability of the perturbative expansion. We show in Figs. 11–14 three-dimensional plots of the cross section and the corresponding K-factors as functions of the factorization and renormalization scales. Notice that as we move from LO to higher orders the curvature of the corresponding surfaces for the cross sections change from negative to positive, showing the presence of a plateau when the scales are approximately equal.

5.4 Stability and the choice of the scales

The issue of determining the best of values of m_H, $\mu_{\rm F}$ and $\mu_{\rm R}$ in the prediction of the total cross section is a rather important one for Higgs searches at LHC. We have therefore detailed in Figs. 8 and 9a our study of the behavior of our results varying the renormalization scale $\mu_{\rm R}$ at a fixed value of the ratio between $\mu_{\rm F}$ and m_H. In these figures we have chosen two values for the ratio between these two scales. Apart from the LO behavior of the scalar cross section, which is clearly strongly dependent on the variation of both scales (see Fig. 8a and d) and does not show any sign of stability since the cross section can be drastically lowered by a different choice of $\mu_{\rm F}$, both the NLO and the NNLO predictions show instead a clear region of local stability for $\mu_{\rm R} > \mu_{\rm F}$ but not too far away from the "coincidence region" $\mu_{\rm F} = \mu_{\rm R} = m_H$. This can be illustrated more

Table 9. Values of the cross sections and K-factors for the scalar Higgs production at the LHC as a function of $\sqrt{S}$ with $\mu_{\rm F} = 2m_H$, with $\mu_{\rm F}^2 = (1/2)\mu_{\rm R}^2$ and $m_H = 114\,{\rm GeV}$. MRST inputs have been used

$\sqrt{S}$	$\sigma_{\rm LO}$	$\sigma_{\rm NLO}$	$\sigma_{\rm NNLO}$	$K^{\rm NLO}$	$K^{\rm NNLO}$
2.0	0.3549	1.031	1.446	2.905	1.403
2.5	0.6393	1.707	2.286	2.670	1.339
3.0	1.003	2.503	3.242	2.496	1.295
3.5	1.439	3.398	4.292	2.361	1.263
4.0	1.945	4.377	5.418	2.250	1.238
4.5	2.515	5.428	6.610	2.158	1.218
5.0	3.146	6.542	7.857	2.079	1.201
5.5	3.834	7.711	9.151	2.011	1.187
6.0	4.575	8.927	10.49	1.951	1.175
6.5	5.367	10.19	11.86	1.899	1.164
7.0	6.207	11.48	13.27	1.850	1.156
7.5	7.093	12.82	14.70	1.807	1.147
8.0	8.023	14.18	16.16	1.767	1.140
8.5	8.994	15.57	17.65	1.731	1.134
9.0	10.00	16.99	19.15	1.699	1.127
9.5	11.05	18.43	20.68	1.668	1.122
10.0	12.14	19.89	22.22	1.638	1.117
10.5	13.26	21.37	23.78	1.612	1.113
11.0	14.41	22.87	25.35	1.587	1.108
11.5	15.60	24.39	26.93	1.563	1.104
12.0	16.82	25.92	28.53	1.541	1.101
12.5	18.07	27.46	30.14	1.520	1.098
13.0	19.35	29.02	31.76	1.500	1.094
13.5	20.65	30.59	33.39	1.481	1.092
14.0	21.99	32.18	35.03	1.463	1.089

Table 10. Values of the cross sections and K-factors for the scalar Higgs production at the LHC as a function of $\sqrt{S}$ with $\mu_{\rm F} = (1/2)m_H$, with $\mu_{\rm F}^2 = (1/2)\mu_{\rm R}^2$ and $m_H = 114\,{\rm GeV}$. MRST inputs have been used

$\sqrt{S}$	$\sigma_{\rm LO}$	$\sigma_{\rm NLO}$	$\sigma_{\rm NNLO}$	$K^{\rm NLO}$	$K^{\rm NNLO}$
2.0	0.6960	1.600	1.830	2.299	1.144
2.5	1.198	2.579	2.862	2.153	1.110
3.0	1.814	3.708	4.028	2.044	1.086
3.5	2.531	4.956	5.300	1.958	1.069
4.0	3.341	6.303	6.661	1.887	1.057
4.5	4.234	7.734	8.096	1.827	1.047
5.0	5.204	9.234	9.593	1.774	1.039
5.5	6.243	10.80	11.14	1.730	1.031
6.0	7.347	12.41	12.74	1.689	1.027
6.5	8.512	14.07	14.38	1.653	1.022
7.0	9.732	15.77	16.06	1.620	1.018
7.5	11.00	17.50	17.77	1.591	1.015
8.0	12.33	19.26	19.50	1.562	1.012
8.5	13.69	21.06	21.26	1.538	1.009
9.0	15.11	22.88	23.05	1.514	1.007
9.5	16.56	24.72	24.86	1.493	1.006
10.0	18.05	26.58	26.69	1.473	1.004
10.5	19.58	28.45	28.53	1.453	1.003
11.0	21.14	30.35	30.39	1.436	1.001
11.5	22.74	32.26	32.26	1.419	1.000
12.0	24.37	34.18	34.15	1.403	0.9991
12.5	26.03	36.12	36.05	1.388	0.9981
13.0	27.72	38.07	37.96	1.373	0.9971
13.5	29.44	40.02	39.89	1.359	0.9968
14.0	31.19	41.99	41.82	1.346	0.9960

simply using Fig. 8b as an example, where we have set the incoming energy of the p–p collision at 14 TeV. In this case, for instance, we have chosen $m_H = \mu_{\rm F} = 100\,{\rm GeV}$ ($C = 1$), and it is clear from the plots that a plateau is present in the region of $\mu_{\rm R} \sim 130\,{\rm GeV}$. Similar trends are also clearly visible at NNLO, though the region of the plateau for the scalar cross section is slightly wider. Also in this case it is found that the condition $\mu_{\rm R} > \mu_{\rm F}$ generates a reduced scale dependence. Away from this region the predictions show a systematic scale dependence, as shown also for the choice of $C = 1/2$ in the remaining figures. In Fig. 9 we repeat the same study for the K-factors, relaxing the condition on the coincidence of all the scales and plotting the variations of $K^{\rm NLO}$ and $K^{\rm NNLO}$ in terms of $\mu_{\rm R}$. In the case $m_H = \mu_{\rm F} = 100\,{\rm GeV}$ the plateau is reached for $\mu_{\rm R} \sim 150\,{\rm GeV}$ for $K^{\rm NLO}$ and $\mu_{\rm R} \sim 200\,{\rm GeV}$ for $K^{\rm NNLO}$. In the first case the NLO corrections amount to an increase by 100 per cent compared to the LO result, while the NNLO corrections modify the NLO estimates by about 20% (MRST). Similar results are obtained also for $\mu_{\rm F} = 50\,{\rm GeV}$. In this case, at the plateau, the NLO corrections are still approximately 100% compared to the LO result and the NNLO corrections increase this value by around 15% (MRST).

5.5 Energy dependence

The energy dependence of the NNLO predictions for the total cross sections and the corresponding K-factors at the LHC are shown in Figs. 15–17, where we have varied the ratio $C = \mu_{\rm F}/m_H$ and $k = \mu_{\rm R}^2/\mu_{\rm F}^2$ in order to illustrate the variation of the results. The cross sections increase sharply with energy and the impact of the NNLO corrections is significant. The K-factors, in most of the configurations chosen, vary between 1 and 2.2. We have chosen the MRST input. The behavior of the K-factors is influenced significantly by the choice of the ratio (k) between $\mu_{\rm R}$ and $\mu_{\rm F}$. In particular, in Fig. 16 the NNLO K-factors increase with $\sqrt{S}$ for $k = 2$, the center of mass energy, which is not found for other choices of scales. The case $k = 1/2$ is close in behavior to the coincident case $\mu_{\rm R}^2 = \mu_{\rm F}^2$. The overall stability of the K-factors is clearly obtained with the choice $k = 1$. We have finally included in Tables 2–10 our numerical predictions in order to make them available to the experimental collaborations.

6 Conclusions

A study of the NNLO corrections to the cross section for Higgs production has been presented. We have implemented the exact three-loop splitting functions in our own parton evolution code. We used as initial conditions (at small scales) the boundary values of Martin, Roberts, Thorne and Stirling and of Alekhin. This study shows that the impact of these corrections are important for the discovery of the Higgs and for a reconstruction of its mass.

The condition of stability of the perturbative expansion is also quite evident from these studies and suggests that the optimal choice to fix the arbitrary scales of the theory are near the coincidence point, with μ_R in the region of a plateau. The determination of the plateau has been performed by introducing in the perturbative expansion and in the evolution a new independent scale (μ_R), whose variation allows one to accurately characterize the properties of the expansion in a direct way.

While this paper was being completed several authors have presented studies of the total Higgs cross section based on threshold resummation of soft or soft-plus-virtual logarithms [27–29]. Our work is based on exact NNLO partonic cross sections. Another relevant paper which recently appeared is [30].

Acknowledgements. The work of A.C., C.C. and M.G. is partly supported by INFN and by MIUR. Numerical studies have been performed using the INFN-LE computational cluster. The work of J.S. was supported in part by the National Science Foundation grant PHY-0354776.

References

1. S. Moch, J. Vermaseren, A. Vogt, Nucl. Phys. B **688**, 101, (2004); Nucl. Phys. B **691**, 129 (2004)
2. V. Ravindran, J. Smith, W.L. van Neerven, Nucl. Phys. B **665**, 325 (2003)
3. W. Van Neerven, A. Vogt, Nucl. Phys. B **603**, 42 (2001); Nucl. Phys. B **588**, 345 (2000)
4. S. Catani, D. de Florian, M. Grazzini, P. Nason, JHEP **07**, 028 (2003)
5. R.V. Harlander, W.B. Kilgore, Phys. Rev. Lett. **88**, 201 801 (2002)
6. C. Anastasiou, K. Melnikov, Nucl. Phys. B **646**, 220 (2002)
7. S. Dawson, hep-ph/9411325
8. V. Ravindran, J. Smith, W.L. Van Neerven, Nucl. Phys. B **704**, 332 (2005)
9. K.G. Chetyrkin, Bernd A. Kniehl, M. Steinhauser, Nucl. Phys. B **510**, 61 (1998)
10. M. Krämer, E. Laenen, M. Spira, Nucl. Phys. B **511**, 523 (1998)
11. K.G. Chetyrkin, B.A. Kniehl, M. Steinhauser, W.A. Bardeen, Nucl. Phys. B **535**, 3 (1998)
12. G. Rossi, Phys. Rev. D **29**, 852 (1984)
13. W. Giele et al., hep-ph/0204316
14. A. Cafarella, C. Corianò, Comput. Phys. Commun. **160**, 213 (2004)
15. A. Cafarella, C. Corianò, M. Guzzi, Nucl. Phys. B **748**, 253 (2006) [hep-ph/0512358]
16. T. Gehrmann, E. Remiddi, Comput. Phys. Commun. **141**, 296 (2001)
17. E. Remiddi, J.A.M. Vermaseren, Int. J. Mod. Phys. A **15**, 725 (2000)
18. A. Vogt, Comput. Phys. Commun. **170**, 65 (2005)
19. O.V. Tarasov, A.A. Vladimirov, A.Y. Zharkov, Phys. Lett. B **93**, 429 (1980)
20. S.A. Larin, J. Vermaseren, Phys. Lett. B **303**, 334 (1993)
21. T. van Ritbergen, J.A.M. Vermaseren, S.A. Larin, Phys. Lett. B **400**, 153 (1997)
22. M. Buza, Y. Matiounine, J. Smith, W.L. van Neerven, Eur. Phys. J. C **1**, 301 (1998)
23. A. Chuvakin, J. Smith, Comput. Phys. Commun. **143**, 257 (2002)
24. A.D. Martin, R.G. Roberts, W.J. Stirling, R.S. Thorne, Eur. Phys. J. C **23** (2002) 73; Phys. Lett. B **531**, 216 (2002)
25. S.I. Alekhin, Phys. Rev. D **68**, 014 002 (2003)
26. A.D. Martin, R.G. Roberts, W.J. Stirling, R.S. Thorne, Eur. Phys. J. C **28**, 455 (2003)
27. S. Moch, A. Vogt, Phys. Lett. B **631**, 48 (2005)
28. E. Laenen, L. Magnea, Phys. Lett. B **632**, 270 (2006)
29. A. Idilbi, X. Ji, J.-P. Ma, F. Yuan, Phys. Rev. D **73**, 077 501 (2006)
30. C. Anastasiou, K. Melnikov, F. Petriello, Phys. Rev. D **72**, 097 302 (2005)
31. W. Giele et al., Les Houches 2001, Physics at TeV colliders, 275, hep-ph/0204316
32. H.L. Lai et al., Eur. Phys. J. C **12**, 375 (2000)
33. K.G. Chetyrkin, B.A. Kniehl, M. Steinhauser, Phys. Rev. D. **79**, 2184 (1997)
34. T. van Ritbergen, J.A.M. Vermaseren, S.A. Larin, Phys. Lett. B **400**, 37 (1997)